

See discussions, stats, and author profiles for this publication at: <https://www.researchgate.net/publication/49814463>

A new chiral, poly-imidazole N-8-ligand and the related di- and tri-copper(II) complexes: synthesis, theoretical modelling, spectroscopic properties, and biomimetic stereoselective...

ARTICLE in DALTON TRANSACTIONS · FEBRUARY 2011

Impact Factor: 4.2 · DOI: 10.1039/c0dt00669f · Source: PubMed

CITATIONS

13

READS

30

8 AUTHORS, INCLUDING:



[Laura Santagostini](#)

University of Milan

35 PUBLICATIONS 753 CITATIONS

[SEE PROFILE](#)



[K. Kristoffer Andersson](#)

University of Oslo

166 PUBLICATIONS 3,425 CITATIONS

[SEE PROFILE](#)



[Maria francesca Iozzi](#)

University of Oslo

21 PUBLICATIONS 409 CITATIONS

[SEE PROFILE](#)



[Giorgio Zoppellaro](#)

Palacký University of Olomouc

74 PUBLICATIONS 1,167 CITATIONS

[SEE PROFILE](#)

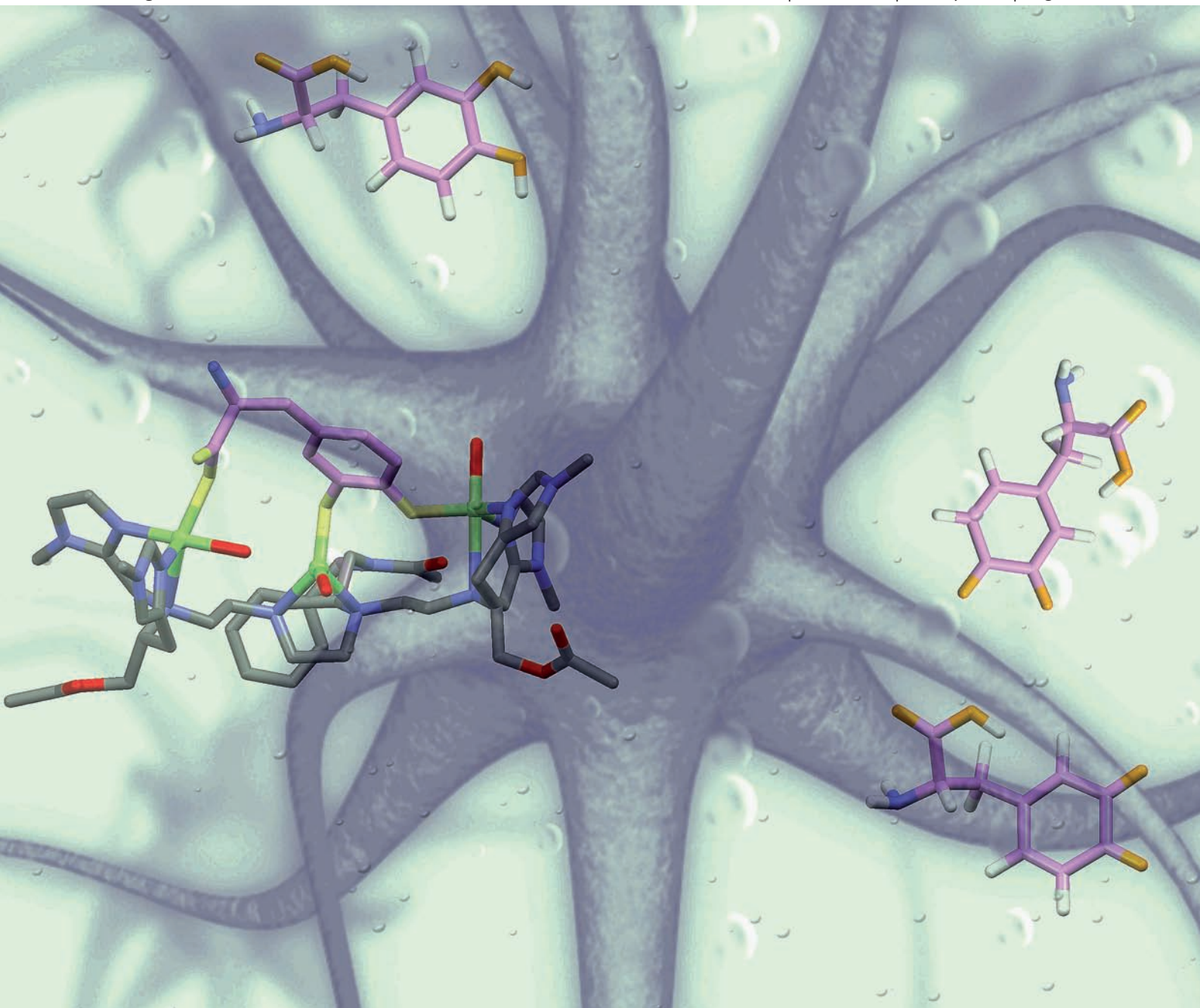
Dalton Transactions

An international journal of inorganic chemistry

www.rsc.org/dalton

Volume 40 | Number 20 | 28 May 2011 | Pages 5365–5632

Celebrating
40 years



ISSN 1477-9226

RSC Publishing

COVER ARTICLE

Gullotti, Zoppellaro *et al.*
A new chiral, poly-imidazole N_8 -ligand
and the related di- and tri-copper(II)
complexes



International Year of
CHEMISTRY
2011



1477-9226(2011)40:20;1-Y

Cite this: *Dalton Trans.*, 2011, **40**, 5436

www.rsc.org/dalton

PAPER

A new chiral, poly-imidazole N₈-ligand and the related di- and tri-copper(II) complexes: synthesis, theoretical modelling, spectroscopic properties, and biomimetic stereoselective oxidations†

Francesco G. Mutti,^{‡a} Michele Gullotti,^{*a} Luigi Casella,^b Laura Santagostini,^a Roberto Pagliarin,^c K. Kristoffer Andersson,^d Maria Francesca Iozzi^e and Giorgio Zoppellaro^{*d}

Received 16th June 2010, Accepted 14th December 2010

DOI: 10.1039/c0dt00669f

The new poly-imidazole N₈ ligand (*S*)-2-piperazinemethanamine-1,4-bis[2-((*N*-(1-acetoxy-3-(1-methyl-1*H*-imidazol-4-yl))-2-(*S*)-propyl)-(1-methyl-1*H*-imidazol-2-ylmethyl))ethyl]-*N*-(phenylmethyl)-*N*-(acetoxy), also named (*S*)-Pz-(C2-(HisIm))₂ (**L**), containing three chiral (*S*) centers, was obtained by a multi-step synthesis and used to prepare dinuclear [Cu₂(**L**)]⁴⁺ and trinuclear [Cu₃(**L**)]⁶⁺ copper(II) complexes. Low-temperature EPR experiments performed on [Cu₂(**L**)]⁴⁺ demonstrated that the two *S* = ½ centers behaved as independent paramagnetic units, while the EPR spectra used to study the trinuclear copper complex, [Cu₃(**L**)]⁶⁺, were consistent with a weakly coupled three-spin ½ system. Theoretical models for the two complexes were obtained by DFT/RI-BP86/TZVP geometry optimization, where the structural and electronic characteristics nicely supported the EPR experimental findings. In addition, the theoretical analysis unveiled that the conformational flexibility encoded in both [Cu₂(**L**)]⁴⁺ and [Cu₃(**L**)]⁶⁺ arises not only from the presence of several σ-bonds and the bulky residues attached to the (*S*)-Pz-(C2-(HisIm))₂ ligand scaffold, but also from the poor coordination ability of the tertiary amino groups located in the ligand side-chains containing the imidazole units towards the copper(II) ions. Both the dinuclear and trinuclear complexes are efficient catalysts in the stereoselective oxidation of several catechols and flavonoid compounds, yielding the corresponding quinones. The structural features of the substrate–catalyst adduct intermediates were assessed by searching the conformational space of the molecule through MMFF94/Monte Carlo (MMFF94/MC) methods. The conformational flexibility of the bound ligand in the complexes proves to be beneficial for substrate binding and recognition. For the dinuclear complex, chiral recognition of the optically active substrates derives from weak electrostatic interactions between bound substrates and folded regions of the ligand scaffold. For the trinuclear complex, in the case of *L*/*D*-Dopa, the chiral recognition has a remarkable stereoselectivity index of 75%, the highest so far reported for this type of reaction. Here the dominant contribution to stereoselectivity arises from the direct interaction between a donor group (the Dopa carboxylate) far from the substrate reaction site (the catechol ring) with the additional (third) copper center not involved in the oxidative catalysis. On the other hand, in the case of bulky substrates, such as *L*/*D*-catechin, the observed poor substrate recognition is associated with much weaker interactions between the chiral regions of the complex and the chiral part of the substrate.

^aDipartimento di Chimica Inorganica, Metallorganica e Analitica “Lamberto Malatesta”, Università di Milano, Istituto ISTM-CNR, Via Venezian 21, 20133, Milano, Italy. E-mail: michele.gullotti@unimi.it, laura.santagostini@unimi.it

^bDipartimento di Chimica Generale, Università di Pavia, Via Taramelli 12, 27100, Pavia, Italy. E-mail: bioinorg@unipv.it

^cDipartimento di Chimica Organica e Industriale, Università di Milano, Via Golgi 19, 20133, Milano, Italy. E-mail: roberto.pagliarin@unimi.it

^dDepartment of Molecular Biosciences, University of Oslo, N0316, Oslo, Norway. E-mail: giorgio.zoppellaro@imbv.uio.no, k.k.andersson@imbv.uio.no, giorgio.zoppellaro@imbv.uio.no

^eThe Center of Theoretical and Computational Chemistry (CTCC), Department of Chemistry, University of Oslo, N0315, Oslo, Norway. E-mail: m.f.iozzi@kjemi.uio.no

† Electronic supplementary information (ESI) available: Listings of plots of the rate constant *versus* substrate concentration for the chiral catechols tested in the [Cu₂(**L**)]⁴⁺ and [Cu₃(**L**)]⁶⁺, the cartesian coordinates (xyz) or pdb format of the optimized structure for [Cu₂(**L**)(OH)₄], [Cu₂(**L**)]⁴⁺(H₂O)₄, [Cu₃(**L**)(OH)₆] and [Cu₃(**L**)]⁶⁺(H₂O)₆ copper complexes obtained by DFT/RI-BP86/TZVP calculations and the neutral adducts [Cu₂(**L**)-*L*-Dopa](OH)₂, [Cu₂(**L**)-*D*-catechin](OH)₂ and [Cu₃(**L**)-*L*-Dopa](OH)₃ obtained by DFT/RI-BP86/def2-SV(P) calculation. See DOI: 10.1039/c0dt00669f

‡ Present address: Department of Chemistry, Organic and Bioorganic Chemistry, University of Graz, Heinrichstrasse 28, 8010 Graz, Austria. E-mail: francesco.mutti@uni-graz.at

Introduction

Aerobic oxidation of many natural organic substrates is performed *in vivo* by multicopper enzymes, whose active site contains a dinuclear or a trinuclear metal cluster.^{1–3} For instance, tyrosinase, also known as polyphenol oxidase,^{4–6} contains a dinuclear copper center (type 3) and exhibits both monooxygenase and oxidase activities. In the monooxygenase activity, the enzyme catalyzes an oxygen atom insertion into the C–H bond *ortho* to the phenol hydroxyl group yielding an *ortho*-quinone, whereas in the oxidase activity two molecules of an *ortho*-diphenol are oxidized to *ortho*-diquinone. Other related enzymes, like the catechol oxidase from *Ipomoea batatas*,^{7–9} exhibit only oxidase activity. The presence of a trinuclear type 2–type 3 copper cluster embedded in the protein backbone characterizes enzymes like laccase,¹⁰ ascorbate oxidase,¹¹ and bilirubin oxidase,^{12–14} all of which contain an additional type 1 (blue) copper center¹⁵ and for this reason are addressed in the literature as multicopper “blue” oxidases.¹⁶ Biologically, the plant enzymes belonging to this family couple the one-electron oxidation of electron-rich aromatic substrates like catechols with the four-electron reduction of dioxygen to water,^{15,17–21} whereas enzymes from other sources perform different functions. For example, the serum protein ceruloplasmin is involved in the metabolism of Cu and Fe and exhibits ferroxidase activity in the same way as the yeast protein Fet3p.²² Structural data are available for some of the blue oxidases,^{23–31} but the intimate nature of the activated oxygen intermediate(s) produced within the catalytically competent trinuclear copper center still remains a matter of debate.^{32–41}

Mimicking the properties and reactivity of such versatile enzymatic systems, with either dinuclear^{42–48} or trinuclear^{49–55} copper clusters, through synthetic design is a challenging task that requires the unveiling of the link between structure and function.^{56,57} A synthetic approach to the trinuclear clusters is particularly difficult, as it involves the assembly of a suitable polydentate ligand containing eight nitrogen donors, engineered in a fashion that can replicate the distribution of the octa-histidyl ligands among the type 2 and type 3 copper centers.^{58–66} Moreover, the artificial biomimetic system needs to be catalytically functional, and hence capable of performing, for instance, the oxidation of phenols or catechols^{61–66} using dioxygen, and hopefully following a reaction pathway similar to that of blue oxidases. Finally, since metalloenzymes often promote asymmetric catalysis *in vivo*, due to the steric constraints induced by the molecular scaffold, such structural properties can also be implemented in the design of chiral biomimetic systems, to exploit the potential of molecular recognition in the catalytic process. While several biomimetic models able to replicate the structural and electronic features of strongly coupled dinuclear^{42–48} or trinuclear copper centers^{49–55} have been reported, it is still a challenge to rationalize the factors (structural and electronic) which need to be translated into the synthetic metallo-organic scaffold in order to perform stereoselective oxidation of substrates. From a biological perspective, steric factors and stereospecific interactions of the substrate with protein amino acid residues (*e.g.* electrostatic interactions, H-bonding) close to the metal active site provide the basis for substrate chiral discrimination. However, these factors are the result of a complex molecular organization, and thus they are hard to engineer into a much simpler synthetic complex.

So far the application of chiral biomimetic copper complexes to the stereoselective oxidation of exogenous substrates has met with limited success, and this largely results from the synthetic challenge associated with the synthesis of large, polyfunctional ligand molecules.^{45,56–57} For a long time our group has been developing synthetic functional models containing dinuclear and trinuclear copper centers and some interesting results in the stereoselective catalytic oxidation of L-/D-Dopa and their derivatives were obtained using the chiral complexes [Cu₃(PHI)](ClO₄)₆^{61,62} and [Cu₂((*S*)-DABN-3Bz₄)](ClO₄)₄.⁶³ Interestingly, in the first case the performance of the trinuclear complex was superior to that of the corresponding dinuclear complex, while in the latter case the reverse was true, with the dinuclear complex acting as a better stereoselective catalyst, due to the different mechanisms of substrate recognition prevailing in the two cases.³

As in principle trinuclear, type 2–type 3 complexes can provide more versatile and rich catalytic properties, our efforts to further improve the efficiency and molecular recognition ability of the copper biomimetic complexes led to the synthesis of a new octadentate nitrogen ligand containing three chiral centers (*S*)-Pz-(C2-(HisIm))₂ (**L**) (Chart 1). This ligand contains a central piperazine residue acting as the didentate binding unit for the type 2 Cu coordination site (Site B), connected to two *N*-ethyl chains carrying L-histidine/imidazole tridentate moieties as terminal groups, with the aim of mimicking the type 3 Cu coordination environment (Sites A). Two chiral centers are located close to the CuA sites, in a similar fashion as in the previously developed ligand PHI (Chart 1).^{58,61–63} In addition, a third chiral center has been introduced into the piperazine spacer, with the bulky *N*-benzyl-*N*-ethylacetamide residue, which opens up the possibility of further modification of the ligand in the future. For instance, an additional Cu type 1-like site could be linked to this chain, which could potentially lead to the assembly of a complete tetranuclear model of the copper blue oxidases. Herein we describe the synthesis of ligand **L** and its dinuclear and trinuclear copper(II) complexes, and

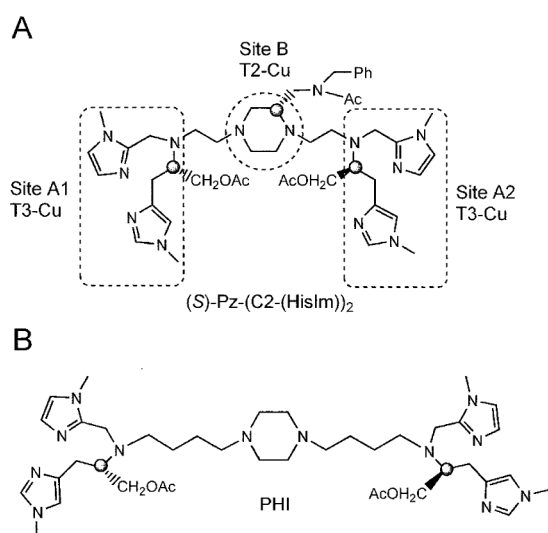


Chart 1 (A) Molecular sketch of the structure of the ligand (*S*)-Pz-(C2-(HisIm))₂ highlighting the different coordination sites for copper(II) ions (Site A1, A2 and B). (B) Structure of the ligand PHI. The positions of the chiral carbon centers are highlighted in the chemical drawings by circles.

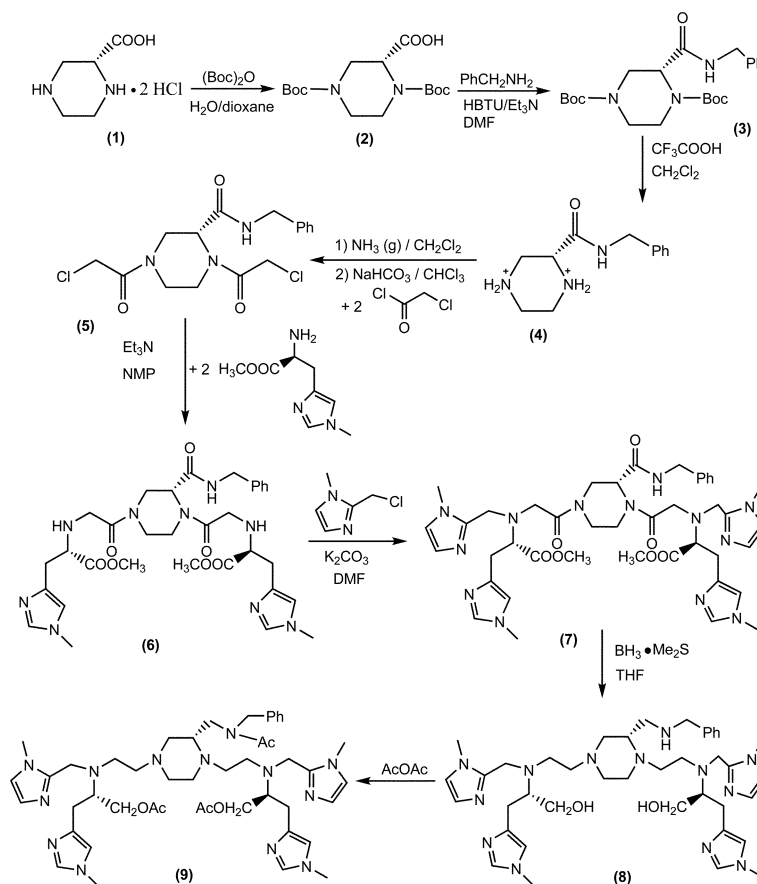
the investigation of their spectromagnetic properties, theoretically derived structures, and stereoselective catalytic oxidation of several catechol and flavonoid compounds.

Results

Synthesis of the ligand and of the corresponding di- and trinuclear copper complexes

The synthetic steps involved in the preparation of the chiral N_8 -ligand (*S*)-Pz-(C2-(HisIm))₂, carrying the biologically relevant imidazole donors in the chelating arms, are reported in Scheme 1. Due to the high insolubility of the starting material, (*S*)-piperazine carboxylic acid dihydrochloride (**1**), in all organic solvents, it was initially protected with Boc, by overnight reaction at room temperature in water–dioxane mixture (1 : 1, v/v) (yield 77%). The so formed derivative (**2**), which was recrystallized from benzene–*n*-hexane, reacted slowly (3 d) under rigorous anaerobic conditions with benzylamine, even in the presence of HBTU as a condensing reagent, but afforded after aqueous work-up and flash chromatography purification the related amide (**3**) in good yield (89%). Deprotection of **3** from Boc, allowed formation of compound **4** in quantitative yield; this was then suspended in CH_2Cl_2 and gaseous ammonia was bubbled for 30 min until the free amino groups were obtained. Those groups were then subjected to condensation with chloroacetyl chloride under Groszkowski conditions. The reaction occurred slowly (~2 d) and required consecutive additions of small

aliquots of reactant in order to obtain an effective conversion into the diacetylated compound (**5**). However, such a procedure proved to be very effective and **5** was formed almost quantitatively. This intermediate was then subjected to a condensation reaction with *N*¹-methyl-L-histidine methyl ester, which gave compound **6** in a reasonable yield (38%), where the chiral arms containing the *N*-methylimidazole donors are connected to the ancillary amino groups of the piperazine moiety. Then, further condensation of **6** with *N*-methylchloromethyl imidazole provided **7** in a better yield (46%). Compounds **6** and **7** were both obtained as orange oils that needed careful chromatographic purification (SiO_2 and Al_2O_3). Compound **7** was reduced to the amide functionalities by $\text{BH}_3 \cdot \text{Me}_2\text{S}$, giving the intermediate **8** (yield 78%), which was finally acetylated, affording the ligand (*S*)-Pz-(C2-(HisIm))₂ (**9**, **L**) as yellow oil (yield 37%). All compounds **1–9** were completely characterized by chemical analyses and spectroscopic methods (^1H NMR, ^{13}C NMR, ESI-MS, UV-Vis, polarimetric and CD techniques). The ESI-MS spectra of all the compounds showed good agreement with the simulated spectra, together with additional clusters of peaks corresponding to the adduct with a sodium ion, which was always present in the medium. The related copper complexes were then synthesized from **9** dissolved in MeCN by addition of the appropriate amount of copper(II) perchlorate in methanol. The products were first precipitated by cooling the reaction mixture in an ice bath. After filtration, the products were finally purified by repeated washings of the pale green-grey powders with diethyl ether, until analytically pure



Scheme 1 Synthetic route for the ligand (*S*)-Pz-(C2-(HisIm))₂.

products were obtained. All the attempts made to obtain crystals of the dinuclear and trinuclear copper complexes suitable for X-ray analysis turned out to be unsuccessful and gave formation of aggregates at best, despite the large number of different environmental conditions probed (concentration changes, mixed solvents, different counterions, temperature gradients); for this reason, we tried to derive alternative structural information about the complexes by theoretical calculations (*vide infra*).

Electronic and CD spectra

The electronic and CD spectra of $[\text{Cu}_2(\text{L})]^{4+}$ and $[\text{Cu}_3(\text{L})]^{6+}$ (Fig. 1 and 2) closely resemble those of the parent copper(II) complexes derived from the PHI ligand.⁵⁸ The near-UV region of the optical spectra shows a well defined shoulder of moderate intensity on the tail of the strong UV absorption, centered in the range 280–300 nm. The CD spectra exhibit a peak of positive sign near the wavelength of the UV shoulder, and a negative peak below 250 nm. Careful inspection of the CD profile in this high energy region shows the presence of two components, the spectra of $[\text{Cu}_2(\text{L})]^{4+}$ and $[\text{Cu}_3(\text{L})]^{6+}$ share a negative peak at 224 nm, but the former exhibits a stronger negative component at 213 nm, while for the latter this feature is clearly inverted, even though the curve does not cross the *x*-axis. As discussed previously,⁵⁸ the origin of the bands below 300 nm must be of charge-transfer type within the copper(II)-imidazole and copper(II)-amine chromophores, as the ligand is transparent in the near-UV/Vis region. In particular, the electronic bands in the range 210–230 nm are due to $\sigma(\text{imidazole}) \rightarrow \text{Cu}(\text{II})$ LMCT transitions,⁵⁸ and therefore different CD behavior in this range reflects differences in the relative orientations of the Cu(II)-imidazole chromophores

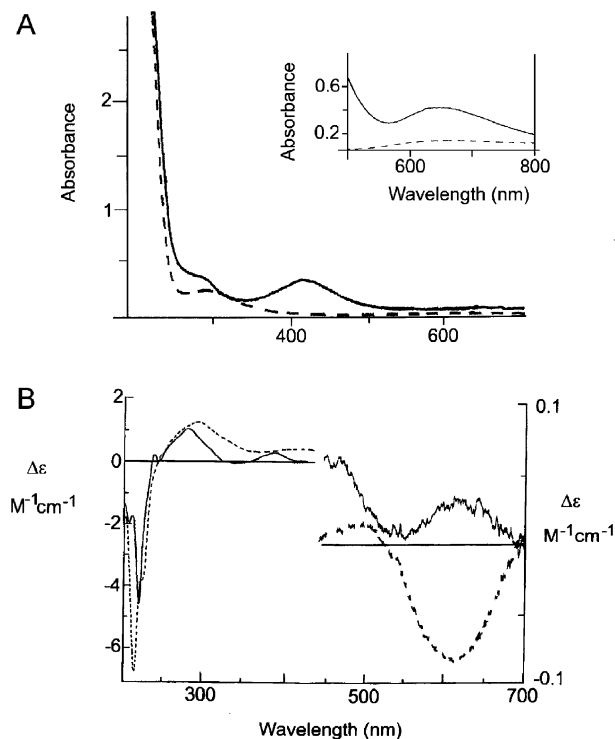


Fig. 1 (A) Electronic and (B) CD spectra of $[\text{Cu}_2(\text{L})]^{4+}$ (---) and $[\text{Cu}_2(\text{L})(\text{N}_3)_3]^{2+}$ (—) in MeCN–MeOH 9 : 1 (v/v) solution at $T = 293$ K. The inset shows the expanded region of the d–d transitions.

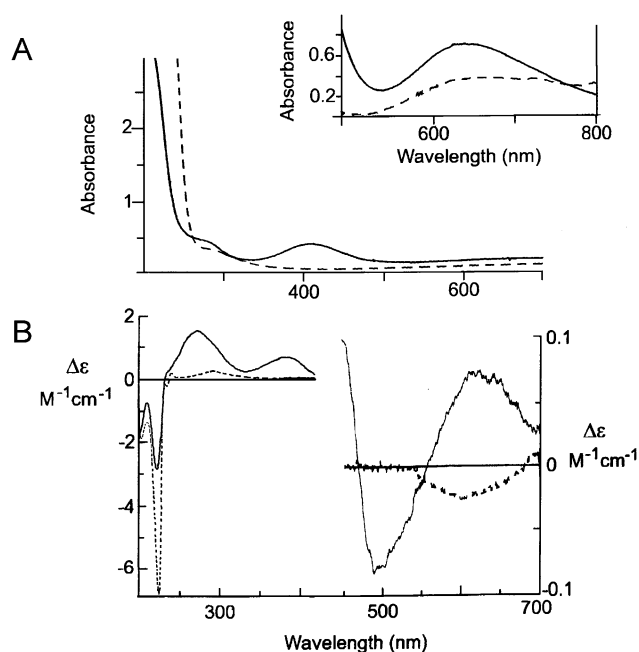


Fig. 2 (A) Electronic and (B) CD spectra of $[\text{Cu}_3(\text{L})]^{6+}$ (---) and $[\text{Cu}_3(\text{L})(\text{N}_3)_3]^{3+}$ (—) in MeCN–MeOH 9 : 1 (v/v) solution at $T = 293$ K. The inset shows the expanded region of the d–d transitions.

in the $[\text{Cu}_2(\text{L})]^{4+}$ and $[\text{Cu}_3(\text{L})]^{6+}$ complexes. In the visible region, a weak and broad absorption extending from 550 to beyond 800 nm encompasses the Cu^{II} d–d transitions, but the better resolution of the CD spectra enables us to distinguish the spectra of the two complexes. For $[\text{Cu}_2(\text{L})]^{4+}$ two bands of opposite sign at 486 nm (positive) and 614 nm (negative) are clearly resolved, while for $[\text{Cu}_3(\text{L})]^{6+}$ only the negative component at 614 is present but the CD profile features positive optical activity above 690 nm. In general, the similarity of the absorption spectra of $[\text{Cu}_2(\text{L})]^{4+}$ and $[\text{Cu}_3(\text{L})]^{6+}$ indicates that, as in the PHI series,⁵⁸ the Cu^{II} center bound to the piperazine site (CuB) provides a minor contribution to the spectra.

As shown in Fig. 1 and 2, the addition of azide ions to solutions of $[\text{Cu}_2(\text{L})]^{4+}$ and $[\text{Cu}_3(\text{L})]^{6+}$ results in the growth of an intense LMCT band near 410 nm and a marked increase in intensity of the LF band, with a broad maximum in the range between 600 and 650 nm. The 410 nm band is due to the $\pi(\text{N}_3^-) \rightarrow \text{Cu}^{\text{II}}$ LMCT transition and its symmetric shape indicates that azide binds in the terminal mode to the copper(II) centers in all cases,^{67,68} whereas bridging azide typically gives rise to characteristic multicomponent LMCT bands.⁶⁹ The LMCT band is apparently associated with weak and slightly blue-shifted CD activity. This is in striking contrast with the behavior of the parent $[\text{Cu}_2(\text{PHI})]^{4+}$ and $[\text{Cu}_3(\text{PHI})]^{6+}$ complexes, where the azide– Cu^{II} LMCT bands generated prominent exciton couplets in the CD spectra.⁶² Coupling between the transition dipole moments of the azide– Cu^{II} LMCT bands could occur because of their relative spatial proximity in the azide adducts of the Cu–PHI complexes, whereas here the $\text{Cu}^{\text{II}}\text{--N}_3^-$ chromophores are further apart and non-interacting. Interestingly, in the d–d region the Cotton effect for the ~600 nm band of the azide adducts is reversed with respect to the precursor copper(II) complexes. This indicates that azide reduces the conformational mobility of the ligand and causes a

change from the preference for the λ conformation of the histidine chelate ring in the CuA sites to a preference for the δ conformation in the corresponding azide adducts.^{61,62}

The dinuclear $[\text{Cu}_2(\text{L})]^{4+}$ complex binds azide with rather high affinity and it is interesting to note that only two azide molecules can bind to these centers, because only two steps can be separated in the optical titration, and saturation occurs after the addition of nearly two equiv. azide, with no further observable spectral changes upon addition of even a very large excess of this ligand. The two steps can be separated and the binding constants estimated from the spectrophotometric assay. The shape of the absorption band developing on formation of the adducts is similar in each step, but it is still possible to distinguish the steps by the presence of different isosbestic points in the two titration ranges, so that the binding constants can be estimated. In the range of $[\text{N}_3^-]:[\text{Cu}_2]$ ratios of 0.0 to 1.0, the isosbestic point is detected at 350 nm and the equilibrium constant, obtained from a double reciprocal plot was determined as $K_1 = 6400 \text{ M}^{-1}$. In the range of $[\text{N}_3^-]:[\text{Cu}_2]$ ratios of 1.1 to 2.1, the isosbestic point occurred at 346 nm, and the equilibrium constant was determined as $K_2 = 5800 \text{ M}^{-1}$. The Hill equation was also used for determination of the equilibrium constant and stoichiometry of the adduct to confirm the data obtained from the double reciprocal plot. The values of $K_1 = 6400 \text{ M}^{-1}$ and $K_2 = 5700 \text{ M}^{-1}$ and Hill coefficients $n_1 = 1.02$ and $n_2 = 1.08$ were in agreement with the former results. Azide binding experiments were also performed with the trinuclear complex $[\text{Cu}_3(\text{L})]^{6+}$, with the observed growth of the LMCT being quite similar to that of the dinuclear complex. However, in this case it was not possible to separate the process into three binding steps. Due to the fact that saturation occurs after the addition of three equiv. azide, and that the intensity of the LMCT band is larger than that obtained for $[\text{Cu}_2(\text{L})]^{4+}$, we assume that three azide molecules bind with high affinity to $[\text{Cu}_3(\text{L})]^{6+}$.

EPR experiments and analysis for the $[\text{Cu}_2(\text{L})][\text{ClO}_4]_4$ system

The EPR measurements on the dinuclear complex $[\text{Cu}_2(\text{L})]^{4+}$ and its adducts with azide and L-Dopa were carried out in diluted glassy solution ($10^{-3} \text{ dm}^3 \text{ mol}^{-1} \text{ cm}^{-1}$, MeCN–MeOH, 9 : 1 v/v). The observed EPR resonances and their computer simulated envelopes are shown in Fig. 3a and Fig. 3d as solid and broken lines respectively. The derived spin-Hamiltonian parameters and the estimated spin concentrations are collected together in Table 1. Although $[\text{Cu}_2(\text{L})]^{4+}$ contains two copper(II) ions caged in the ligand framework, the recorded EPR spectrum (Fig. 3a, solid line) shows two nearly uncorrelated $S = \frac{1}{2}$ spin centers. The spin-Hamiltonian parameters obtained through spectral simulation gave $g_{zz} = 2.238(4)$, $g_{yy} = g_{xx} = 2.066(2)$ and Cu^{II} hyperfine term $A_{zz} = 146 \pm 5 \times 10^{-4} \text{ cm}^{-1}$. These values are typically found in Cu^{II} systems embedded in a (slightly) distorted tetragonal field,^{70–74} and are different from those obtained earlier for the parent complex $[\text{Cu}_2(\text{PHI})]^{4+}$ ($g_{zz} = 2.231$, $g_{yy} = g_{xx} = 2.071$, and $A_{zz} = 167 \times 10^{-4} \text{ cm}^{-1}$).^{61,62} Moreover, the spin-Hamiltonian parameters are more consistent with a set of 2N/2O donors rather than three N-donors, according to the empirical relation between g_{zz}/A_{zz} described earlier by Peisach and Blumberg.⁷⁵ It is worth noting that the slightly broadened resonance envelope, as clearly seen along the g_{zz} (i.e. g_{\parallel}) component of the spectrum indicates the presence of very weak dipolar interactions between metal centers

in the frozen matrix solution.^{76,77} The EPR spectrum recorded at cryogenic temperature ($T = 3.6 \text{ K}$) did not exhibit significant changes in the overall EPR envelope (Fig. 4a) and no $\Delta m_s = 2$ transition could be detected. It showed only a very minor reduction in the total spin concentration ($S_T = 1.8$). The EPR spectrum recorded for the adduct obtained after addition of two azide equivalents to $[\text{Cu}_2(\text{L})]^{4+}$ is shown in Fig. 3d (solid line). The coordination of azide molecules to the Cu^{II} ions do not alter the negligible interaction between the two spin $S = \frac{1}{2}$ units, with the spin-Hamiltonian parameters at $g_{zz} = 2.231(3)$, $g_{yy} = 2.079(2)$, and $g_{xx} = 2.038(2)$ and the Cu^{II} hyperfine term ($A_{zz} = 153 \pm 3 \times 10^{-4} \text{ cm}^{-1}$). Therefore, the exogenous N_3^- groups should adopt the terminal binding mode for both Cu^{II} centers, in agreement with the UV/vis/CD fingerprints discussed above, and such a behavior mirrors that found for the $[\text{Cu}_2(\text{PHI})]^{4+}$ complex upon N_3^- binding.^{61,62}

The catecholase activity of the complex was probed by reacting a slight excess (1.2 equiv.) of L-Dopa with $[\text{Cu}_2(\text{L})]^{4+}$, in a strictly maintained oxygen free MeCN–MeOH solution, with the additional presence of a small excess of MBTH (2.0 equiv.) (MTBH = 3-methyl-2-benzothiazolinone hydrazone). Under these conditions, both the Cu^{II} ions were reduced to Cu^{I} , as substantiated by the lack of paramagnetic signals in the resulting EPR spectrum, this being accompanied by development of the Dopa-ortho-quinone-MBTH band in the optical spectrum. Therefore, during turnover complex $[\text{Cu}_2(\text{L})]^{4+}$ undergoes structural changes, from an “open” conformational arrangement which most probably characterizes the substrate-free complex, where the Cu^{II} ions are located far apart to each other (*vide infra*), to a “folded” conformation, where a favorable interaction can occur between the substrate (L-Dopa) and both CuA centers.

EPR experiments and analysis for the $[\text{Cu}_3(\text{L})][\text{ClO}_4]_6$ system

The EPR analysis of the trinuclear complex $[\text{Cu}_3(\text{L})]^{6+}$ and its adducts was carried out in diluted glassy solution ($2 \times 10^{-3} \text{ dm}^3 \text{ mol}^{-1} \text{ cm}^{-1}$, MeCN–MeOH 9 : 1 v/v) in a similar manner as that described previously for the parent $[\text{Cu}_2(\text{L})]^{4+}$ system. The derived spin-Hamiltonian parameters and spin concentrations are also included in Table 1. The observed EPR resonance for the complex, recorded at $T = 77 \text{ K}$ (Fig. 3b, solid line) is very broad and poorly resolved because of the large line-width tensor components. Therefore, only the averaged hyperfine tensor components associated with the three metal ions ($A_{zz} = 145 \pm 7 \times 10^{-4} \text{ cm}^{-1}$, $A_{yy,xx} = 20 \times 10^{-4} \text{ cm}^{-1}$) and the estimated averaged g-tensor values could be obtained from computer simulations (Fig. 3b, dashed-dotted line) as $g_{zz} = 2.233(5)$, $g_{yy} = 2.092(3)$, $g_{xx} = 2.081(2)$. Thus, these parameters are not much different from those obtained for the other chiral trinuclear copper complex $[\text{Cu}_3(\text{PHI})]^{6+}$ ($g_{zz} = 2.232$, $g_{yy} = g_{xx} = 2.070$, and $A_{zz} = 166 \times 10^{-4} \text{ cm}^{-1}$),^{61,62} and closely resemble those observed for the dinuclear complex $[\text{Cu}_2(\text{L})]^{4+}$. The calculated spin concentration at $T = 77 \text{ K}$ accounts for ~ 1.7 spins, hence much less than three uncorrelated $S = \frac{1}{2}$ centers. The presence of the forbidden $\Delta m_s = 2$ transition at half-field ($g_{av} = 4.27$, Fig. 3c), although very weak, highlights the occurrence of triplet-state species ($S = 1$) within the system. However, the one-third $\Delta m_s = 3$ transition, which would constitute a clear fingerprint for the presence of quartet states ($S = 3/2$), was not detected even by employing very high microwave power (100 mW). Increasing

Table 1 Spin-Hamiltonian parameters (g , A) and spin concentration (S_T) calculated for the dinuclear and trinuclear copper complexes and their related adducts (with azide and L-Dopa)

	$[\text{Cu}_2(\text{L})]^{4+}$		$[\text{Cu}_2(\text{L})(\text{N}_3)_2]^{2+}$	
g_{zz}	2.238(4)		2.231(3)	
g_{yy}	2.066(2)		2.079(2)	
g_{xx}	2.066(2)		2.038(2)	
A_{zz}	$146 \pm 5 \times 10^{-4} \text{ cm}^{-1}$		$153 \pm 3 \times 10^{-4} \text{ cm}^{-1}$	
A_{yy}	$14 \pm 2 \times 10^{-4} \text{ cm}^{-1}$		$10 \pm 2 \times 10^{-4} \text{ cm}^{-1}$	
A_{xx}	$14 \pm 2 \times 10^{-4} \text{ cm}^{-1}$		$9 \pm 2 \times 10^{-4} \text{ cm}^{-1}$	
L/G^a	0.63		0.63	
LW_x^b	$84 \times 10^{-4} \text{ cm}^{-1}$		$34 \times 10^{-4} \text{ cm}^{-1}$	
LW_y^b	$130 \times 10^{-4} \text{ cm}^{-1}$		$102 \times 10^{-4} \text{ cm}^{-1}$	
LW_z^b	$88 \times 10^{-4} \text{ cm}^{-1}$		$62 \times 10^{-4} \text{ cm}^{-1}$	
S_T^c	1.96 ± 0.12		1.85 ± 0.11	
	$[\text{Cu}_3(\text{L})]^{6+}$		$[\text{Cu}_3(\text{L})(\text{N}_3)_3]^{3+}$	
g_{zz}	2.233(5)		2.231(2)	
g_{yy}	2.092(3)		2.081(2)	
g_{xx}	2.081(2)		2.035(2)	
A_{zz}	$145 \pm 7 \times 10^{-4} \text{ cm}^{-1}$		$152 \pm 3 \times 10^{-4} \text{ cm}^{-1}$	
A_{yy}	^d n.d.		$19 \pm 3 \times 10^{-4} \text{ cm}^{-1}$	
A_{xx}	^d n.d.		$9 \pm 2 \times 10^{-4} \text{ cm}^{-1}$	
L/G^a	1.00		0.67	
LW_x^b	$93 \times 10^{-4} \text{ cm}^{-1}$		$34 \times 10^{-4} \text{ cm}^{-1}$	
LW_y^b	$159 \times 10^{-4} \text{ cm}^{-1}$		$102 \times 10^{-4} \text{ cm}^{-1}$	
LW_z^b	$103 \times 10^{-4} \text{ cm}^{-1}$		$65 \times 10^{-4} \text{ cm}^{-1}$	
S_T^c	1.74 ± 0.11		1.20 ± 0.08	
	$[\text{Cu}_3(\text{L})(\text{N}_3)_3]^{3+}$		$[\text{Cu}_3(\text{L})]^{6+} + \text{L-Dopa}^e$	
	Cu(1)	Cu(2)		
g_{zz}	2.243(2)	2.430(2)	2.232(3)	
g_{yy}	2.081(2)	2.086(1)	2.074(1)	
g_{xx}	2.036(2)	2.086(1)	2.054(1)	
A_{zz}	$153 \pm 5 \times 10^{-4} \text{ cm}^{-1}$	$102 \pm 3 \times 10^{-4} \text{ cm}^{-1}$	$144 \pm 3 \times 10^{-4} \text{ cm}^{-1}$	
A_{yy}	$18 \pm 2 \times 10^{-4} \text{ cm}^{-1}$	$17 \pm 1 \times 10^{-4} \text{ cm}^{-1}$	$19 \pm 2 \times 10^{-4} \text{ cm}^{-1}$	
A_{xx}	$10 \pm 2 \times 10^{-4} \text{ cm}^{-1}$	$17 \pm 1 \times 10^{-4} \text{ cm}^{-1}$	$15 \pm 1 \times 10^{-4} \text{ cm}^{-1}$	
L/G^a	0.70	0.67	0.67	
LW_x^b	$34 \times 10^{-4} \text{ cm}^{-1}$	$32 \times 10^{-4} \text{ cm}^{-1}$	$65 \times 10^{-4} \text{ cm}^{-1}$	
LW_y^b	$103 \times 10^{-4} \text{ cm}^{-1}$	$24 \times 10^{-4} \text{ cm}^{-1}$	$130 \times 10^{-4} \text{ cm}^{-1}$	
LW_z^b	$66 \times 10^{-4} \text{ cm}^{-1}$	$30 \times 10^{-4} \text{ cm}^{-1}$	$56 \times 10^{-4} \text{ cm}^{-1}$	
$S_T^{c,f}$	2.35 ± 0.13		0.85 ± 0.05	

^a L/G indicates the Lorentzian/Gaussian line-shape. ^b $LW_{x,y,z}$ indicates the line-width tensor. ^c S_T indicates the total Spin-concentration calculated against $\text{Cu(II)}-\text{EDTA}$ standard, 1.0 mM. ^d Not determined; the values of $A_{yy,xx}$ of $20 \times 10^{-4} \text{ cm}^{-1}$ have been arbitrarily used and fixed without variation in the EPR spectra simulation as upper limits for the hyperfine $\langle xx \rangle$ and $\langle yy \rangle$ components. ^e Recorded under anaerobic conditions in the presence of MBTH. Note that the corresponding dinuclear copper complex $[\text{Cu}_2(\text{L})]^{4+}$ was EPR silent under the same reaction conditions. ^f The best ratio obtained for the double-integrated EPR simulated envelope of Cu(1) vs. Cu(2) was 1.15.

the sample temperature (to 120 K) led to an even broader and unresolved spectrum, accompanied by a slight increase in the total spin-concentration ($S_T \sim 2.0 \pm 0.1$). The EPR spectrum recorded at the lowest possible temperature obtainable with our instrumental set-up ($T = 3.6 \text{ K}$, Fig. 4b) was very similar to the spectrum recorded at $T = 77 \text{ K}$ and exhibited a more resolved $\Delta m_s = 2$ transition (Fig. 4c), but again no $\Delta m_s = 3$ transition could be detected. Furthermore, the total amount of spin, calculated along the $\Delta m_s = 1$ resonance line, around $g = 2$, was only slightly smaller than that extracted at higher temperatures ($S_T \sim 1.5$). As shown in Fig. 4d, the double integration of the $\Delta m_s = 2$

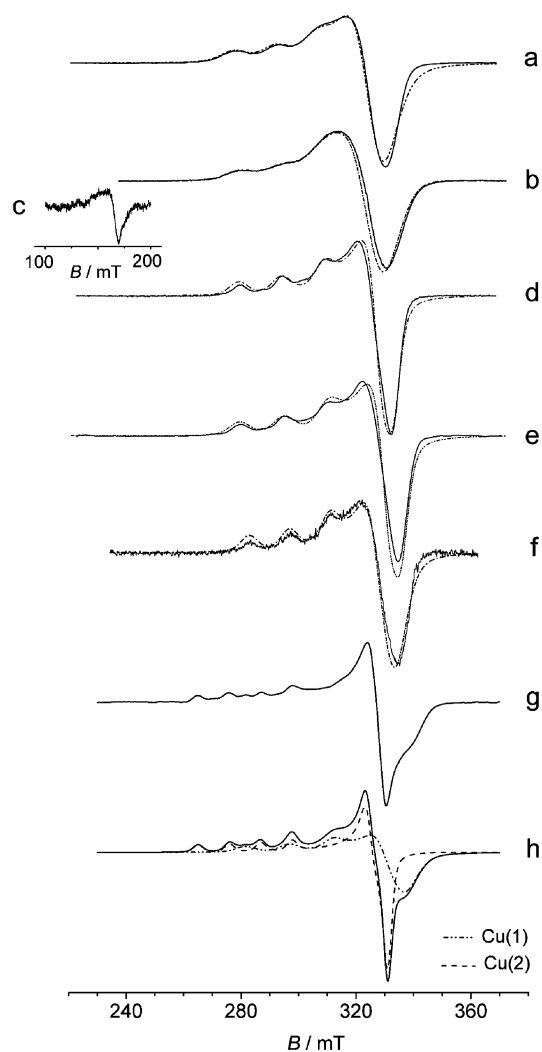


Fig. 3 The X-band EPR spectra (solid lines) and their computer simulation envelopes (broken lines) obtained for the dinuclear $[\text{Cu}_2(\text{L})]^{4+}$ and trinuclear $[\text{Cu}_3(\text{L})]^{6+}$ copper complexes. (a) $[\text{Cu}_2(\text{L})]^{4+}$ and (d) its bis-azide adduct; (b) $[\text{Cu}_3(\text{L})]^{6+}$, (c) the $[\text{Cu}_3(\text{L})]^{6+}$ half-field transition, (e) $[\text{Cu}_3(\text{L})]^{6+}$ plus 1 equiv. of N_3^- , (g) $[\text{Cu}_3(\text{L})]^{6+}$ plus 3 equiv. of N_3^- and (h) its computer simulation showing the overlapped features of two copper species (Cu1 and Cu2); (f) $[\text{Cu}_3(\text{L})]^{6+}$ after reaction with L-Dopa (in presence of MBTH). Experimental parameters: (a) 9.572 GHz frequency, (b) 9.580 GHz frequency, (c) 9.582 GHz frequency, (d) 9.571 GHz frequency, (e) 9.571 GHz frequency, (f) 9.570 GHz frequency, (g) 9.571 GHz frequency. Then, 100 kHz modulation frequency, 0.7 mT modulation amplitude, 82 ms time constant, 168 s sweep time, $T = 77 \text{ K}$, 4–6 scans accumulated and averaged, power 0.20 mW in (a), 0.32 mW in (d), 0.40 mW in (b),(e) and (g), (c) 8.0 mW (12 scans), and 0.1 mW in (f).

signal against the root of applied microwave power ($\chi_{\text{EPR}}, DI/\sqrt{P}$) increases by decreasing the sample temperature T , according to the Curie-law ($\chi_{\text{EPR}} = C/T$), but the product $\chi_{\text{EPR}} \times T$ remains almost constant. This result clearly indicates that there is no thermal population or depopulation of high spin states ($S = 1$, $S = 3/2$) in the temperature range examined ($3.6 \text{ K} \leq T \leq 31 \text{ K}$), and those must remain in equilibrium with each other, according to the Boltzman distribution.⁷⁶ However, it is also clear from these results that dipolar and exchange terms are to some extent stronger in the trinuclear complex than in the dinuclear

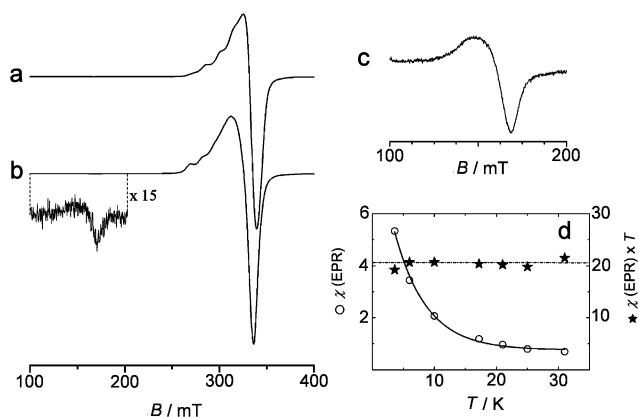


Fig. 4 The X-band EPR spectra obtained at $T = 3.6$ K for: (a) the dinuclear complex $[\text{Cu}_2(\text{L})]^{4+}$ ($1.0 \times 10^{-3} \text{ dm}^3 \text{ mol}^{-1} \text{ cm}^{-1}$ in MeCN–MeOH 9 : 1, v / v) and (b) the trinuclear complex $[\text{Cu}_3(\text{L})]^{6+}$ ($2.0 \times 10^{-3} \text{ dm}^3 \text{ mol}^{-1} \text{ cm}^{-1}$ in MeCN–MeOH 9 : 1, v / v). Panel (c) shows the $\Delta m_s = 2$ transition observed in the spectrum of $[\text{Cu}_3(\text{L})]^{6+}$ recorded at the same temperature but using higher microwave power. (d) Temperature dependence of the χ_{EPR} (○, arbitrary units) and $\chi_{\text{EPR}} \times T$ (★), obtained from the double-integrated $\Delta m_s = 2$ transition divided by the square root of the applied microwave power ($\chi_{\text{EPR}} = DI/\sqrt{P}$), in the low temperature region ($T = 3.6\text{--}31$ K). The solid line shows the Curie-law behavior and the dashed-dotted line the $\chi_{\text{EPR}} \times T = C$ (with C being the Curie constant). Experimental parameters: (a) 9.664, (b) 9.666, and (c) 9.666 GHz frequency; all spectra recorded at 100 kHz modulation frequency, 57 dB gain, 0.7 mT modulation amplitude, 82 ms time constant, 168 s sweep time; with 1 scan for (a) and (b), and 4 scans for (c). Microwave power was 0.016 mW in both (a) and (b), and 2.00 mW in (c).

complex and these interactions arise from a closer through-space proximity of the three metal ions. This will be demonstrated by theoretically modelling the solution structure and electronic properties of $[\text{Cu}_3(\text{L})][\text{ClO}_4]_6$ (*vide infra*).

After the addition of one azide equiv. to the complex solution (*i.e.* $[\text{N}_3^-]:[\text{Cu}_3(\text{L})]^{6+} = 1:1$), the EPR spectrum shows a better resolved resonance envelope (Fig. 3e, solid line) as compared to the free trinuclear complex. Here, the derived spin-Hamiltonian parameters are consistent with one tetragonal and almost isolated copper center ($g_{zz} = 2.231(2)$, $g_{yy} = 2.081(2)$, $g_{xx} = 2.035(2)$, $S_T = 1.20 \pm 0.08$). The N_3^- group, in this instance, should promote conformational changes in the trinuclear copper structure, binding one of the two CuA sites in a terminal fashion and forcing the remaining two copper ions (the other CuA and CuB) to (antiferromagnetically) interact even more strongly, such that at $T = 77$ K the $S = 0$ state for the CuA–CuB pair is nearly fully populated. Upon further addition of azide molecules (3 equiv. in total), the resulting low temperature EPR spectrum clearly shows the presence of two different types of copper coordination environments (Fig. 3g, solid line). These are recognized through spectrum simulation as: (i) a (slightly) distorted tetragonal Cu^{II} ion, marked as Cu(1) in Fig. 3h (dashed–dotted line), with $g_{zz} = 2.243(2)$ and $A_{zz} = 153 \pm 5 \times 10^{-4} \text{ cm}^{-1}$, and (ii) a second Cu^{II} center marked as Cu(2) in Fig. 3h (dashed line), characterized by larger g_{zz} component (2.430(2)) and featuring a smaller hyperfine term $A_{zz} = 102 \pm 3 \times 10^{-4} \text{ cm}^{-1}$. The combined features of these two species (Fig. 3h solid line) closely resemble the experimentally observed spectrum but highlight an almost one-to-one ratio between these two different Cu^{II} ions ($1.15:1.00 = \text{Cu}(1):\text{Cu}(2)$)

which is supported by the estimated total spin concentration of the adduct ($S_T \sim 2.35$). No forbidden $\Delta m_s = 2$ transition was observed in this case, which, on the other hand, cannot exclude the occurrence of very weak antiferromagnetic interactions among the spin centers. The failure to detect the $\Delta m_s = 2$ signal, or even more the $\Delta m_s = 3$ resonance signal, is not surprising since the transition probabilities of the forbidden transitions depend only on the anisotropic exchange and, as a consequence, for very weakly coupled systems like this azide adduct, they remain undetectable.⁷⁸

The properties of $[\text{Cu}_3(\text{L})]^{6+}$ in the azide binding process strongly differ from those observed previously for $[\text{Cu}_3(\text{PHI})]^{6+}$, where two N_3^- molecules were found to bind as terminal ligands to a single CuA and a third azide group acted as a bridge between the remaining CuA and the CuB center (yielding a system with $S_T = 0.9 \pm 0.1$).⁶² Taking all these results together, complex $[\text{Cu}_3(\text{L})]^{6+}$ shows a significant structural and conformational flexibility, as witnessed by its response to the exogenous molecules binding, which clearly modulate appreciably the magnetic interactions between the $S = \frac{1}{2}$ centers. This brings into question whether the Cu^{II} ions coordinated at the A sites, which provide a set of three *N*-donors, are more “structurally constrained” with respect to the Cu^{II} ion bound to the B site, which contains only two effective *N*-donors. As will be described later on in the theoretical calculations, the conformational flexibility of the trinuclear complex arises not only from the presence of several σ -bonds in the molecular scaffold but also from the weakened coordination capability of the tertiary amino groups located in the two side-arms containing the imidazole ligands. In this case these tertiary amine nitrogens, because of the strain induced on the molecular backbone upon further coordination of a copper at the B site, act as poor donors for the CuA centers. Similar behavior is observed in pyrazole-substituted ethylenediamine–copper(II) complexes,⁷⁹ in (methylbenzimidazolyl)methylamino-*m*-xylene–copper(II) complexes,⁸⁰ as well as in other $\text{Cu}^{\text{I}}/\text{Cu}^{\text{II}}$ model complexes.⁸¹ Furthermore, in $[\text{Cu}_3(\text{L})]^{6+}$ the conformational flexibility of the molecular backbone arises also from the combination of the steric demand of the residues connecting the tertiary *N*-donors, *i.e.* the short *N*-ethyl chains linking the histidine imidazole groups (Site A) to the piperazine unit (Site B), and the presence of bulky groups located near the A and B sites. These structural features together with presence of a copper at the B site, relax the strain present in the complex by opening up the coordination environments, especially in the two sites A.

In a similar manner to the experiment using the dinuclear copper complex, the catecholase activity of the complex was probed by reacting a slight excess (1.2 equiv.) of L-Dopa with $[\text{Cu}_3(\text{L})]^{6+}$ in the presence of MBTH, strictly maintaining oxygen free solutions (MeCN–MeOH). After substrate oxidation, only one type of Cu^{II} remained well defined in the EPR spectrum, with spin-Hamiltonian parameters (see Table 1) consistent with one tetragonal copper (II) ion (Fig. 3f, solid line). It is important to note at this point that these parameters support the hypothesis that this site corresponds to a redox innocent CuA center, because they are analogous to those observed in the binuclear complex $[\text{Cu}_2(\text{L})]^{4+}$ (see Table 2) which contains only CuA centers. Therefore, while only two Cu^{II} emerge as catalytically active, we speculate that those consist of a CuA–CuB pair and the remaining CuA center should contribute to the enhancement of the remarkable stereoselectivity that this complex exhibits in the oxidation of the substrate L-Dopa

Table 2 The computed (DFT/TZVP//BP86 level) spin-density (from Mulliken population analyses) for the two biomimetic copper complexes (neutral forms). Note that for the trinuclear copper complex different spin-configurations have also been included. See Fig. 6B and Fig. 7B for the related atomic labeling

Sites	Mulliken (α - β)				
	[Cu ₂ (L)(OH) ₄] [\uparrow , CuA1] [\uparrow , CuA2]	[Cu ₃ (L)(OH) ₆] [\uparrow , CuA1] [\uparrow , CuB] [\uparrow , CuA2]	[Cu ₃ (L)(OH) ₆] [\uparrow , CuA1] [\uparrow , CuB] [\downarrow , CuA2]	[Cu ₃ (L)(OH) ₆] [\downarrow , CuA1] [\uparrow , CuB] [\uparrow , CuA2]	[Cu ₃ (L)(OH) ₆] [\uparrow , CuA1] [\downarrow , CuB] [\uparrow , CuA2]
CuA1	0.53	0.50	0.50	-0.50	0.50
CuA2	0.54	0.50	-0.50	0.50	0.50
CuB	—	0.46	0.46	0.46	-0.46
N1	0.06	0.00	0.00	0.00	0.00
N2	0.07	0.02	0.02	-0.02	0.02
N3	0.00	0.07	0.07	0.07	-0.07
N4	0.00	0.05	0.05	0.05	-0.05
N5	0.06	0.00	0.00	0.00	0.00
N6	0.05	0.01	-0.01	0.01	0.01
N7	0.00	0.05	0.05	-0.05	0.05
N8	0.00	0.05	-0.05	0.05	0.05
O1	0.13	0.25	0.26	-0.26	0.26
O2	0.19	0.17	0.17	-0.17	0.17
O3	0.19	0.21	0.21	0.21	-0.21
O4	0.16	0.19	0.19	0.19	-0.19
O5	—	0.28	-0.28	0.28	0.28
O6	—	0.16	-0.16	0.16	0.16

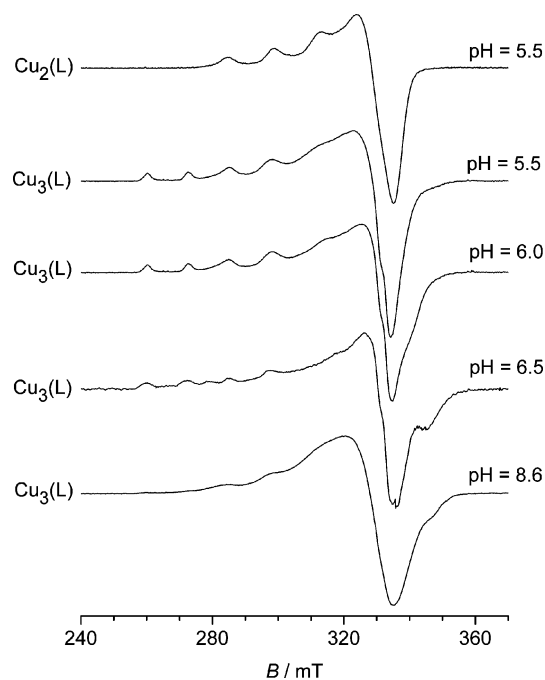


Fig. 5 The X-band EPR spectra obtained for the dinuclear [Cu₂(L)]⁴⁺ and trinuclear [Cu₃(L)]⁶⁺ copper complexes at various pH (MeOH–PBS buffer). Experimental parameters: 9.572–9.581 GHz frequency, 100 kHz modulation frequency, 0.7 mT modulation amplitude, 82 ms time constant, 168 s sweep time, $T = 77$ K, 2–4 scans accumulated and averaged, power 0.32–0.60 mW.

(*vide infra*). Since the investigations of the catalytic properties of the complex were carried out in methanol–phosphate buffer solution (PBS, pH = 8.6), the pH dependency of the EPR signal has been followed, in addition, from the alkaline to acid environment (MeOH–PBS buffer). While in basic frozen solution (Fig. 5) the EPR signal of [Cu₃(L)]⁶⁺ mirrored that observed in MeOH–CH₃CN (Fig. 3b) but with an additional small resonance signal

around 345 mT ($g < 2$), when the acidity of the medium increased the presence of multiple species became unambiguous. At least two different types of Cu^{II} signals evolved in a narrow pH range ($6.5 < \text{pH} < 6.0$). One copper signal featuring small hyperfine coupling (hfc) ($A_{zz} = 120 \pm 4 \times 10^{-4} \text{ cm}^{-1}$) and another Cu^{II} signal showed larger Cu hfc component ($A_{zz} = 150 \pm 6 \times 10^{-4} \text{ cm}^{-1}$). After comparison with the EPR signature witnessed in the dinuclear copper complex recorded in the same MeOH–PBS solution at pH = 5.5, which contains only CuA sites, the former signal in [Cu₃(L)]⁶⁺ can be clearly assigned as originating from the Cu^{II} bound at the B site. Thus, the findings reinforce the hypothesis of a large conformational mobility of [Cu₃(L)]⁶⁺ in solution, a property that turned out beneficial for substrate conversion, especially with respect to the stereoselective oxidation of L-Dopa into L-dopaquinone.

Theoretically-derived structure for the dinuclear copper complex

The optimized structure (DFT/RI-BP86/TZVP) of the dinuclear complex in the charged [Cu₂(L)(H₂O)₄]⁴⁺ and neutral form [Cu₂(L)(OH)₄] are shown in Fig. 6A and Fig. 6B respectively. The four ClO₄⁻ ions were replaced in the calculation by four water molecules and by four OH⁻ groups. Such a choice in replacing the identity of the anion was made in order to reduce (computationally) the complexity of the present systems whilst keeping the entire ligand framework and to compare, in addition, the geometry of the charged *versus* neutral complexes. Furthermore by looking at the majority of the X-ray structures known for synthetic copper complexes in presence of ClO₄⁻ counter-anions, they are usually rather weakly coordinated to the metal (Cu²⁺–OCIO₃⁻, 2.3–2.9 Å) and within catalysis in MeOH–PBS buffer, solvent molecules (e.g. H₂O/OH) are indeed those filling the coordination sphere of the metal ions. Structurally, the two copper coordination halves are located rather apart from each other, both in the charged (+4) and in the neutral complexes (CuA1–CuA2, $d = 12.82$ Å and $d = 13.16$ Å respectively), as expected, and the “open” arrangement is largely favored, owing to the chair conformation

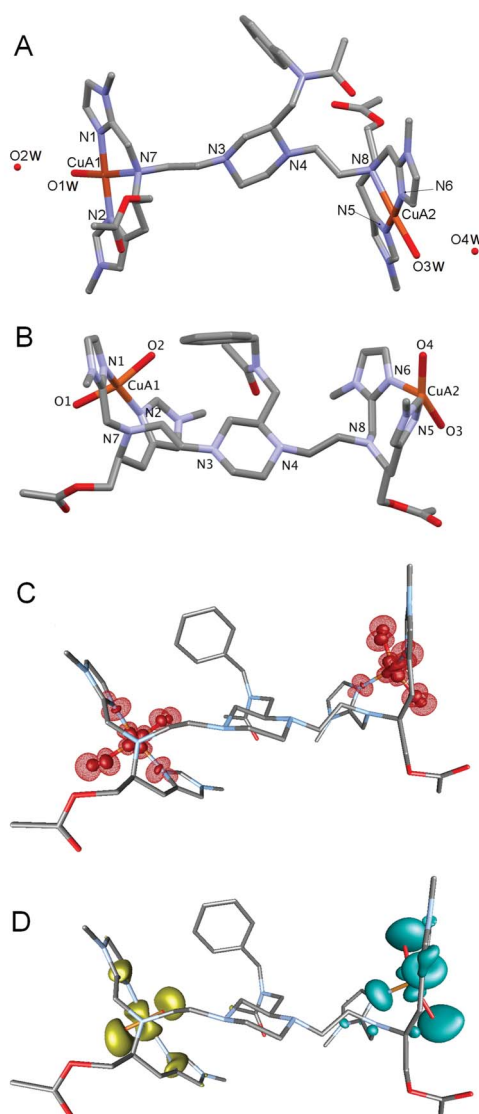


Fig. 6 (A) The optimized geometry (RI-PB86/TZVP) of the charged dinuclear copper complex $[\text{Cu}_2(\text{L})]^{4+}[\text{H}_2\text{O}]_4$. (B) The optimized geometry (RI-PB86/TZVP) of the neutral dinuclear copper complex $[\text{Cu}_2(\text{L})](\text{OH})_4$. Hydrogen atoms were not depicted in (A) and (B) for clarity; (C) The iso-surfaces of the derived spin density in the complex: opaque inner-most and translucent outer-most surfaces correspond to iso-values of 0.020 a.u. and 0.0025 a.u., respectively; (D) The singly-occupied molecular orbitals (SOMOs): the SOMO1 (CuA1) and SOMO2 (CuA2) are illustrated in yellow and blue, respectively. Relevant calculated distances as depicted in (B): Cu(A1)–N1 = 2.067 Å, Cu(A1)–N2 = 2.063 Å, Cu(A1)–N7 = 2.723 Å, Cu(A1)–O1 = 1.922 Å, Cu(A1)–O2 = 1.957 Å, Cu(A2)–N5 = 2.101 Å, Cu(A2)–N6 = 2.091 Å, Cu(A2)–N8 = 3.135 Å, Cu(A2)–O3 = 1.915 Å, Cu(A2)–O4 = 1.917 Å.

adopted by the central piperazine unit. This structural feature prevents participation of the piperazine nitrogen donors (labeled N3 and N4 in Fig. 6A and Fig. 6B) as coordinating groups for the two copper(II) ions. In the same way, the coordination of the other nitrogen donor included in the piperazine side-chain residue (the phenylmethyl-*N*-acetoxy moiety) is also hindered. The optimized geometry of the copper centers evolves from square planar in the charged complex (Fig. 6A), where one water molecule, after

optimization, acts on each Cu^{II} center very weakly (Cu–O2 W and Cu–O4 W, with distances 4.00 Å and 3.90 Å), to distorted tetragonal in the neutral form (Fig. 6B). The copper ligands in the charged complex include the nitrogen donors of the two imidazolyl groups (Cu–N distances 1.94–1.95 Å), the tertiary amino groups (CuA1–N7 and CuA2–N8 distances of 2.29 Å and 2.28 Å respectively) and one equatorial water molecule (Cu–O at 2.09 Å). Similarly, the copper ligands in the neutral form of the complex are provided by the nitrogen donors of the two imidazolyl groups and two hydroxide ions (Cu–N distances from 2.06 to 2.10 Å and Cu–O distances from 1.92 to 1.96 Å). It is interesting to note that the tertiary amino groups belonging to the ethynyl chains act, in this instance, as very weak ligands (Cu–N7, Cu–N8 distances 2.72 and 3.13 Å respectively). Since the catalyses are carried out in a basic environment (pH = 8.6), this form should represent the dominant species present in solution. As mentioned earlier in the EPR analysis, the poor coordination ability of such tertiary amino groups is not unprecedented, since it has been observed in the X-ray structures of copper complexes containing pyrazole/benzimidazole ligands where there is steric hindrance.^{79–81} In the neutral $[\text{Cu}_2(\text{L})(\text{OH})_4]$ form, the angle ρ generated between the N1–CuA1–N2 and O1–CuA1–O2 planes is 86.6° and analogous to the other formed by the N5–CuA2–N6 and O3–CuA2–O4 planes ($\rho = 87.2^\circ$) (see Fig. 6B for labelling). The small geometrical differences between the CuA1 and CuA2 coordination spheres depend upon the closer proximity of the former site to the phenylmethyl-*N*-acetoxy group of the piperazine side chain. The spin-density distribution in the neutral complex is illustrated in Fig. 6C ($\langle S^*S^* \rangle = 2.0027$) and numerical values are reported in Table 2. The latter shows that no spin density is transferred from the metal centers through the spacer and therefore the dipolar term is very small, meaning that the two spin units should behave as nearly independent systems. Similar behavior is present in the charged complex (data not shown). The computational results are thus in harmony with the EPR analysis previously described for this complex. Electronically, the two coordinated coppers feature almost energetically “quasi-degenerate” SOMOs orbitals ($\Delta E(\text{SOMO1} - \text{SOMO2}) = 1.67 \text{ kJ mol}^{-1}$). These frontier orbitals are shown in Fig. 6D, with SOMO1 drawn in yellow and SOMO2 in cyan. As noted above for the features of the geometry, the slight electronic differences between the SOMOs are due to the closer through-space approach of the CuA1 half to the phenylmethyl-*N*-acetoxy residue with respect to the CuA2 half. This residue provides a weak hydrogen bonding interaction between one of its benzyl protons and one of the hydroxo ligands of CuA1 ($\text{H}_{\text{benzyl}}\text{–O2} = 2.39 \text{ Å}$), and such interaction leads to the small rise in the energy of SOMO1 as compared to SOMO2.

Theoretically-derived structure for the trinuclear copper complex

The molecular sketch of the optimized structure (DFT/RI-BP86/TZVP) obtained for the charged $[\text{Cu}_3(\text{L})(\text{H}_2\text{O})_6]^{6+}$ and the neutral complex $[\text{Cu}_3(\text{L})(\text{OH})_6]$ are shown in Fig. 7A and Fig. 7B respectively. Also in this case the perchlorate ions were replaced by six water molecules and six OH[−] groups. Overall, the trinuclear complex in both charged and neutral form adopts a more folded structure with respect to its dinuclear counterpart; this is due to the active participation of the piperazine nitrogen donors in the coordination to the third copper ion (CuB) that dictates a boat

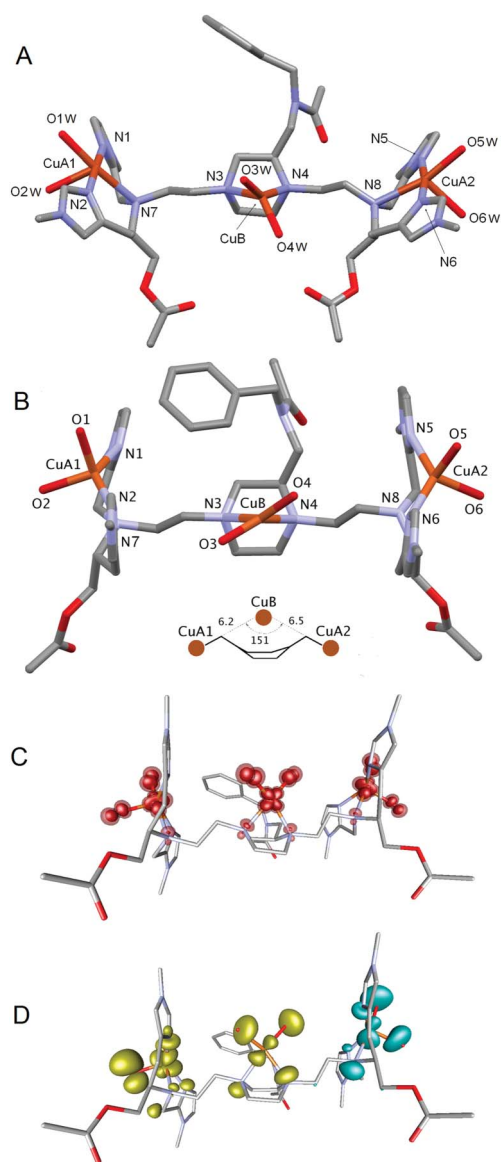


Fig. 7 (A) The optimized geometry (RI-PB86/TZVP) of the charged trinuclear copper complex $[\text{Cu}_3(\text{L})]^{6+}[\text{H}_2\text{O}]_6$. (B) The optimized geometry (RI-PB86/TZVP) of the neutral trinuclear copper complex $[\text{Cu}_3(\text{L})][\text{OH}]_6$. Hydrogen atoms were not depicted in (A) and (B) for clarity. (C) The iso-surface of the derived spin density in the complex: opaque inner-most and translucent outer-most surfaces correspond to iso-values of 0.020 a.u. and 0.0025 a.u., respectively; (D) The singly-occupied molecular orbitals (SOMOs). The two quasi-degenerate SOMO1a (CuA1) and SOMO1b (CuB) are illustrated in yellow, and the SOMO2a (CuA2) in cyan. Relevant calculated distances as depicted in (B): CuA1–N1 = 2.226 Å, CuA1–N2 = 2.081 Å, CuA1–N7 = 2.427 Å, CuA1–O1 = 1.922 Å, CuA1–O2 = 1.969 Å, CuA2–N5 = 2.159 Å, CuA2–N6 = 2.077 Å, CuA2–N8 = 2.518 Å, CuA2–O5 = 1.917 Å, CuA2–O6 = 1.965 Å, CuB–N3 = 2.139 Å, CuB–N4 = 2.182 Å, CuB–O3 = 1.889 Å, CuB–O4 = 1.885 Å.

conformation in the piperazine ring. The presence of CuB results in shorter through-space distances among the three metal centers. Those are computed as slightly elongated in the charged complex (Fig. 7A) where CuA1–CuB = 7.32 Å, CuB–CuA2 = 6.99 Å, CuA1–CuA2 = 14.13 Å, and with a CuA1–CuB–CuA2 bond angle of 161.6°, as compared to the neutral complex (Fig. 7B),

where CuA1–CuB = 6.19 Å, CuB–CuA2 = 6.54 Å, CuA1–CuA2 = 12.36 Å, and the CuA1–CuB–CuA2 bond angle is 151.3°. Both optimized structures suit the strong dipolar broadening observed in the recorded EPR spectrum. From the derived structures it is evident why a closer approach of the three metal ions, such as that resulting from the formation of hydroxo bridge(s) between CuA1 and CuB, is strongly hindered. This effect, as observed already in the modelling of the dinuclear complex, originates from the short dimethylene chains attached to the piperazine linker between the two CuA sites, and the steric hindrance brought by the bulky phenylmethyl-*N*-acetoxy residue connected to the piperazine moiety. In the charged $[\text{Cu}_3(\text{L})(\text{H}_2\text{O})_6]^{6+}$ complex the coordination environment for the CuA sites can be described as slightly distorted square pyramidal, with one of the water molecules weakly interacting with the metal in the axial position (CuA1–O2 W with $d = 3.20$ Å and CuA2–O6 W with $d = 3.15$ Å). The other copper ligands for the CuA sites are given by two histidines, with CuA–N distances within 1.95–1.98 Å, the tertiary amino group from the ethynyl side chain (CuA1–N7 and CuA2–N8, 2.43 Å and 2.54 Å respectively) and the remaining water molecule (CuA1–O1 W and CuA2–O5 W at 2.11 Å and 2.17 Å respectively). The CuB is subject to strong tetragonal field, with CuB–N3 and CuB–N4 distances of 2.19 Å and 2.09 Å respectively, and CuB–O4 W and CuB–O3 W of 2.06 Å and 2.07 Å. In the uncharged $[\text{Cu}_3(\text{L})(\text{OH})_6]^0$ complex (Fig. 7B), a different coordination environment especially for the CuA sites is present, with geometrical parameters similar to those previously described in its dinuclear neutral counterpart. Here, the CuA–N(His) optimized distances are slightly longer (CuA–N = 2.08–2.23 Å) than the mean Cu–ligand bond distances usually observed in copper proteins (His(N ϵ), Cu–N \sim 2.11 Å; His(N δ), Cu–N \sim 2.02 Å),⁸² while the Cu–N distances at the B site (CuB–N \sim 2.15 Å) and the long contact to the tertiary amino nitrogen donor at the A site (CuA–N $_i$ = 2.43–2.52 Å) are analogous to those found in the literature for similar chelating groups containing short aliphatic spacers.^{79–81} The angle ρ generated between the N1–CuA1–N2 and O1–CuA1–O2 planes is 86.1° while the other one formed by the N5–CuA2–N6 and O5–CuA2–O4 planes is 84.5°, hence quite similar to those witnessed in the binuclear complex. The remaining ρ angle formed between the N3–CuB–N4 and O3–CuB–O4 planes is much smaller at 34.1°. The three copper(II) ions are electronically non-equivalent both in the charged and neutral form; as shown in Fig. 7D for the neutral complex, the highest SOMO is localized on the CuA2 site (SOMO2a, cyan contour), while the other two orbitals are distributed across the CuA1 and CuB sites (SOMO1a and SOMO1b respectively, yellow contours) and energetically quasi-degenerate ($\Delta E(\text{SOMO1a} - \text{SOMO1b}) = 1.81$ kJ mol^{–1}). The spin density ($\langle S^*S \rangle = 3.7556$) for the $S = 3/2$ configuration is mostly due to the population of the Cu^{II} $d_{x^2-y^2}$ orbital; nevertheless, a certain amount of spin-density is also transferred to the oxygen and the nitrogen atoms in the metal coordination sphere. This is shown in Fig. 7C, with numerical values reported in Table 2. As depicted by the energy plot in Fig. 8, the quartet-state spin configuration ($S = 3/2$, [\uparrow , CuA1] [\uparrow , CuB] [\uparrow , CuA2]) and the doublet-state spin configurations ($S = 1/2$ states, ([\downarrow , CuA1] [\uparrow , CuB] [\uparrow , CuA2]); [\uparrow , CuA1] [\downarrow , CuB] [\uparrow , CuA2]; [\uparrow , CuA1] [\uparrow , CuB] [\downarrow , CuA2]), obtained by spin-flipping the unpaired spin on the CuA1, CuB and CuA2 centers, were found energetically close to each other, with a small

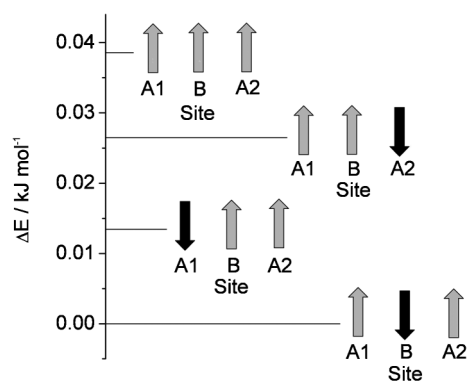
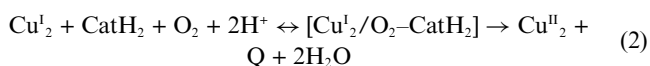
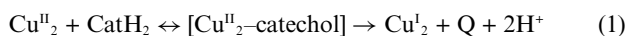


Fig. 8 The relative energies of the different spin configurations available in the neutral trinuclear copper cluster $[\text{Cu}_3(\text{L})](\text{OH})_6$ obtained by spin-flipping the unpaired electron along the CuA1, CuB and CuA2 sites, as derived from DFT (RI-PB86/TZVP) single-point calculations.

preference for the $[\uparrow, \text{CuA1}] [\downarrow, \text{CuB}] [\uparrow, \text{CuA2}]$ spin doublet configuration ($\Delta E_q - \Delta E_d = 3.86 \times 10^{-2} \text{ kJ mol}^{-1}$). Table 2 includes in addition the Mulliken spin population analysis obtained for all the different spin configurations reported above. In the trinuclear copper complex, the exchange coupling interactions are therefore rather weak; however, as experimentally seen from the broad and poorly resolved EPR resonance line exhibited by the complex at low temperature, the exchange terms are still able to generate a spread in g , A and L_w (line-width tensor). Thus, we can only observe an overlap of the resonance features associated with the different spin configurations accessible to the complex, even down to cryogenic temperatures, since all those states remain thermally accessible and thus statistically populated according to the Boltzmann distribution, as it has been experimentally verified.

Stereoselective catecholase activity in the dinuclear and trinuclear copper complexes

We explored the potential of the dinuclear and trinuclear copper complexes towards stereoselective oxidations by choosing a representative set of biogenic catechols,⁸³ L-/D-Dopa, the corresponding methyl esters L-/D-DopaOMe and L-/D-norepinephrine, and the pair of diastereoisomeric flavonoids,⁸⁴ D-catechin and L-epicatechin, which possess a hydroxyl functionality with opposite configuration. The activity was evaluated by monitoring the growth of the absorption band due to the formation of the quinone products trapped as adducts with 3-methyl-2-benzothiazolinone hydrazone (MBTH). As shown by the anaerobic EPR experiments, the reaction of a catechol molecule with either $[\text{Cu}_2(\text{L})]^{4+}$ or $[\text{Cu}_3(\text{L})]^{6+}$ complexes occurs with a fast two-electron transfer process leading to simultaneous reduction of two Cu^{II} centers and formation of quinone. Thus, as for the other complexes of the same family previously investigated,³ a two-step mechanism of catechol oxidation can be hypothesized for the present catalytic reactions:

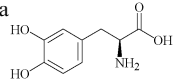
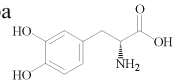
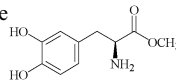
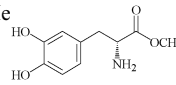
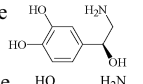
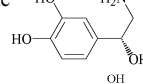
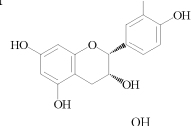
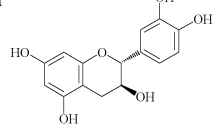


where CatH_2 represents the catechol and Q the quinone. Only in a few cases could the two steps be separated,^{64,68,81,85} i.e. when reaction (1) is much faster than reaction (2), but in general, as in the

present case, the kinetic experiments show monophasic behavior, making it impossible to separate the two steps. For the oxidation of L-/D-Dopa, L-/D-norepinephrine and L-/D-DopaOMe by $[\text{Cu}_2(\text{L})]^{4+}$, the variation of the initial rates of the catalytic oxidations with substrate concentration exhibited a simple hyperbolic behavior and the kinetic parameters could be determined using the Michaelis–Menten equation. On the other hand, the oxidation of D-catechin and L-epicatechin by the same complex showed an inhibition effect at high substrate concentration, and therefore the kinetic parameters had to be estimated using the modified rate eqn (3), which was derived previously.⁸⁵ The $[\text{Cu}_3(\text{L})]^{6+}$ complex behaved according to Michaelis–Menten kinetics with the substrates L-/D-Dopa and L-/D-norepinephrine, whereas with L-/D-DopaOMe, D-catechin and L-epicatechin, inhibition occurred again at high substrate concentration. The dinuclear complex $[\text{Cu}_2(\text{L})]^{4+}$ displays substrate enantio-differentiating ability, as expressed by the $R\%$ index (eqn (4)), in the oxidation of all catechols (Table 3). These stereoselectivity effects are comparable with those previously reported for the Cu complexes derived from chiral binaphthyl and PHI ligands, but the $R\%$ values remain lower than the best values observed in some of those cases.^{63,64} As shown by the EPR analysis and molecular modelling (Fig. 3 and Fig. 6, respectively), in the dinuclear complex the tertiary nitrogen donors connected to the ethynyl chains, especially in basic solutions, very weakly coordinate to the Cu^{II} ions. This is expected to confer enhanced conformational mobility to the two Cu^{II} halves, compared with e.g. $[\text{Cu}_2(\text{PHI})]^{4+}$, where the tertiary nitrogens are coordinated,⁶² and should enable an easier binding of catecholic substrates as bridging ligands, a condition allowing a fast two-electron transfer to the Cu^{II} ions. The stereoselectivity towards L-Dopa observed here is smaller compared, for instance, with that exhibited by the dinuclear complexes containing a chiral dinaphthyl group as the central linker, such as $[\text{Cu}_2((S)\text{-DABN-3Bz}_4)]^{4+}$. In that case, the diamino–dinaphthyl group, connecting the N -donors to longer aliphatic chain spacers (four sp^3 carbons) containing the ancillary methylbenzimidazole units, constituted a more powerful recognition group.^{63,64} When more bulky substrates are considered, L-/D-catechin, the chiral discrimination ability of $[\text{Cu}_2(\text{L})]^{4+}$ is still present, although less prominent ($R\% = 35$).

When the catalytic activity of $[\text{Cu}_3(\text{L})]^{6+}$ is probed, a different behavior is noted, because this complex exhibits the highest enantio-differentiating ability so far reported in the oxidation of L-/D-Dopa, with an $R\%$ index of 75 (Table 4), compared with the $R\%$ index of 61 found for $[\text{Cu}_3(\text{PHI})]^{6+}$.⁶¹ Even in the oxidation of the L-/D-DopaOMe substrates, for which the $R\%$ value is much smaller (21), the recognition capacity of $[\text{Cu}_3(\text{L})]^{6+}$ is much stronger than that exhibited by $[\text{Cu}_3(\text{PHI})]^{6+}$, which is indeed very poor.⁶¹ For both these trinuclear complexes, the observed stereoselectivity depends on K_M , and not on k_{cat} , indicating that it originates from the mode of substrate binding to the tricopper complex. In the productive catalyst–substrate adduct, the catechol residue is thought to bind CuB and one of the CuA centers, as suggested earlier by EPR spectroscopy (see Fig. 3, trace f), and the remaining CuA site may, additionally, provide an anchor for the amino acid portion of L-/D-Dopa.⁶¹ We termed this contribution as *metal induced* discrimination,³ because it depends on the ability of the ancillary metal ion to interact with a substrate group distant from that undergoing the catalytic reaction. This type of recognition mechanism is different from the

Table 3 Kinetic parameters for the stereoselective oxidation of catecholic substrates catalyzed by $[\text{Cu}_2(\text{L})][\text{ClO}_4]_4$ in methanol–50 mM aqueous phosphate buffer, pH 8.6, in the presence of MBTH at 20 °C

Substrate	K_{M} (mM)	k_{cat} (s^{-1})	$k_{\text{cat}}/K_{\text{M}}$ ($\text{M}^{-1} \text{s}^{-1}$)	$R\%^a$	r^{2b}
L-Dopa 	$(5.95 \pm 0.46) \times 10^{-2}$	$(1.42 \pm 0.03) \times 10^{-2}$	239	33	0.99
D-Dopa 	$(1.05 \pm 0.15) \times 10^{-1}$	$(1.28 \pm 0.05) \times 10^{-2}$	122	—	0.97
L-DopaOMe 	$(2.46 \pm 0.14) \times 10^{-2}$	$(3.39 \pm 0.03) \times 10^{-2}$	1380	42	0.99
D-DopaOMe 	$(5.65 \pm 0.63) \times 10^{-2}$	$(3.18 \pm 0.08) \times 10^{-2}$	563	—	0.98
L-norepinephrine 	$(4.75 \pm 0.52) \times 10^{-2}$	$(2.58 \pm 0.06) \times 10^{-2}$	543	21	0.98
D-norepinephrine 	$(4.90 \pm 0.32) \times 10^{-2}$	$(1.72 \pm 0.03) \times 10^{-2}$	352	—	0.99
L-epicatechin ^c 	$(4.51 \pm 0.66) \times 10^{-2}$	$(2.92 \pm 0.17) \times 10^{-2}$	647	35	0.99
D-catechin ^c 	$(1.01 \pm 0.14) \times 10^{-1}$	$(3.12 \pm 0.22) \times 10^{-2}$	310	—	0.98

^a $R\%$ defined in eqn (4) except for norepinephrines and flavonoids, where the L and D suffixes must be inverted. ^b The coefficient of determination (r^2). ^c In methanol–50 mM aqueous phosphate buffer, pH 7.0, with MBTH at 20 °C.

usual *ligand induced* discrimination which is generally provided by chiral complexes in stereoselective catalysis,^{86,87} and is operative also in the catechol oxidation promoted by $[\text{Cu}_2(\text{L})]^{4+}$ and the other dinuclear complexes investigated previously.³ Therefore, the modest enantioselectivity exhibited by $[\text{Cu}_3(\text{L})]^{6+}$ in the catalytic oxidation of L-/D-DopaOMe and the other enantiomeric catechol derivatives could be ascribed to the weaker anchoring ability of the ester group to the remaining CuA center not involved in the substrate oxidation process. When more bulky substrates such as L-/D-catechin are considered, the chiral discrimination featured by $[\text{Cu}_3(\text{L})]^{6+}$ further decreases ($R\% = 16$). The results indicate that the presence of an additional CuA center is not as beneficial to the stereoselective discrimination as in the case of L-/D-Dopa and/or interaction between chiral regions of the ligand with the chiral portion of the substrate become much weakened.

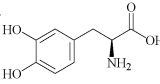
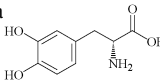
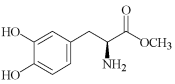
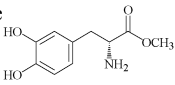
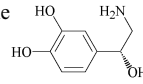
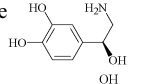
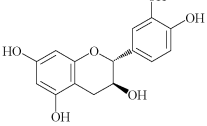
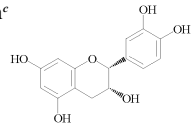
Discussion

Correlation between structural and spectroscopic analyses carried out in several copper proteins exhibiting mono/dioxygenase and/or cresolase activity clearly reveal that the number of copper metal ions caged into the protein backbone cannot be linked straightforwardly with the protein function. Simple mononuclear copper enzymes in fact can exhibit all the types of oxygen activation and substrate oxidation mentioned above. Dinuclear

and magnetically isolated copper centers, such as those present in dopamine β -hydroxylase (DBH),⁸⁸ and peptidylglycine α -hydroxylating monooxygenase (PHM) (where $\text{Cu} \cdots \text{Cu} \approx 11 \text{ \AA}$),⁸⁹ are generally more active towards monooxygenase reactions. On the other hand, dinuclear strongly coupled (antiferromagnetically) copper centers like those characterizing hemocyanin (Hc), tyrosinase (Ty) and catechol oxidase (CO), where the two Cu ions are located much closer to each other (3–4 \AA), can indeed use or activate oxygen very differently.⁴ This reflects the different role of the protein surrounding the metal active site, as the copper ions generate similar Cu_2O_2 peroxy-species in the three proteins. Thus, Hc behaves as an O_2 transport protein, oxyTy can hydroxylate phenols and oxidize catechols, while oxyCO cannot perform monooxygenase reactions but only exhibits catecholase activity.

From the magnetic point of view, because of the negligible interaction between spin units due to the large intramolecular $\text{Cu} \cdots \text{Cu}$ distance ($\sim 13 \text{ \AA}$), the dinuclear $[\text{Cu}_2(\text{L})]^{4+}$ complex reported in this work is more similar to enzymatic systems like DBH and PHM rather than Ty and CO. The trinuclear $[\text{Cu}_3(\text{L})]^{6+}$ complex also bears little similarity (both magnetic and structural) to the trinuclear active site present in the multicopper oxidases, such as laccase and ascorbate oxidase, even though the magnetic interaction between spin units is stronger here than in its dinuclear counterpart. Nevertheless, the potential of these synthetic systems to perform stereoselective catalytic oxidations

Table 4 Kinetic parameters for the stereoselective oxidation of catecholic substrates catalyzed by $[\text{Cu}_3(\text{L})][\text{ClO}_4]_6$ in methanol–50 mM aqueous phosphate buffer, pH 8.6, in the presence of MBTH at 20 °C

Substrate	K_{M} (mM)	k_{cat} (s^{-1})	$k_{\text{cat}}/K_{\text{M}}$ ($\text{M}^{-1} \text{s}^{-1}$)	$\text{R}\%^a$	r^{2b}
L-Dopa 	$(3.84 \pm 0.46) \times 10^{-2}$	$(1.51 \pm 0.04) \times 10^{-2}$	390	75	0.97
D-Dopa 	$(2.48 \pm 0.27) \times 10^{-1}$	$(1.43 \pm 0.06) \times 10^{-2}$	57	—	0.99
L-DopaOMe 	$(9.11 \pm 1.56) \times 10^{-3}$	$(2.14 \pm 0.09) \times 10^{-2}$	2340	21	0.96
D-DopaOMe 	$(1.51 \pm 0.34) \times 10^{-2}$	$(2.32 \pm 0.16) \times 10^{-2}$	1540	—	0.95
D-norepinephrine 	$(3.43 \pm 0.41) \times 10^{-1}$	$(5.45 \pm 0.24) \times 10^{-2}$	160	6	0.99
L-norepinephrine 	$(2.60 \pm 0.37) \times 10^{-1}$	$(3.65 \pm 0.18) \times 10^{-2}$	140	—	0.99
D-catechin ^c 	$(8.06 \pm 1.18) \times 10^{-2}$	$(1.48 \pm 0.10) \times 10^{-1}$	1830	16	0.98
L-epicatechin ^c 	$(1.32 \pm 0.17) \times 10^{-1}$	$(1.77 \pm 0.13) \times 10^{-1}$	1340	—	0.99

^a $\text{R}\%$ defined in eqn (4), except for norepinephrines and flavonoids, where the L and D suffixes must be inverted. ^b The coefficient of determination (r^2).^c In methanol–50 mM aqueous phosphate buffer, pH 7.0, with MBTH at 20 °C.

turned out to be quite remarkable for some substrates. The question that emerges is how the molecular complexity engineered in the organic scaffold (three chiral residues) influences/drives substrate discrimination. Even though the detailed theoretical description of the binding and electron transfer processes in these systems remains outside of the scope of the present work, we noticed that the first step of the catalytic cycle (eqn (1)) implies formation of a $[\text{Cu}^{\text{II}}_2\text{-catechol}]$ complex. In order to explore the conformational space of the molecules, attempts to model the various species were made by adding to the DFT/-BP86/def2-TZVP-derived neutral structure of the complexes the substrates, followed by a simulated annealing process of the adduct, through combination of MMFF94/MC methods. It is important to underline that the MMFF94 force field itself does not account for LFSE (Ligand-Field Stabilization Energy).^{90,91} The lack of such contribution turned out to be quite relevant in the presence of weak donors, such as the piperazine nitrogen coordinating the copper(II) ion at the B site in $[\text{Cu}_3(\text{L})]^{6+}$. Indeed the CuB–N distances became both persistently elongated (2.4–2.6 Å), while the imidazole to copper distances (Cu–N, CuA sites) remained in the range 2.01–2.05 Å, hence close enough to those witnessed in the DFT optimized structures for the substrate free neutral complexes. Hence, the CuB–N distances were kept frozen at 2.18 Å within the conformational search. In modelling the catechol binding step, we assumed that the two OH^- ions were replaced by the catecholato

oxygen donors and binding of both catecholato oxygens to the Cu^{II} metal ions occurred simultaneously. Upon substrate binding, the lowest energy conformers obtained through MMFF94/MC analyses for both L-Dopa and D-catechin, revealed that the overall $[\text{Cu}_2(\text{L})\text{-substrate}](\text{OH})_2$ structures are more folded, compared with the free dinuclear complex, in harmony with the earlier EPR description. The lowest energy conformers obtained in this way were then fully optimized by DFT/RI-BP86/def2-SV(P); as it is shown in the case of $[\text{Cu}_2(\text{L})\text{-L-Dopa}](\text{OH})_2$ illustrated in Fig. 9A, the piperazine residue retains the most stable chair conformation, even in the presence of bound substrate. Here, the phenylmethyl-*N*-acetoxy group tends to fold in such a way as to produce a cavity. This arrangement allows the flat, achiral catecholic portion of L-Dopa to interact easily with the copper(II) ions, hence avoiding steric hindrance. While substrate binding is not sterically hindered, the chiral discrimination exhibited by $[\text{Cu}_2(\text{L})]^{4+}$ towards the dopa substrate appears to be linked to weak electrostatic interactions occurring in the chiral portion of the piperazine residue, namely the phenylmethyl-*N*-acetoxy group, the chiral portion of the substrate and one of the CuA2 *N*-methylimidazole ligands, all located at a distances less than 5 Å from each other. When more bulky substrates are considered, L-/D-catechin, the chiral discrimination of $[\text{Cu}_2(\text{L})]^{4+}$ is associated with analogous sources of weak interactions. The fully optimized structure obtained through DFT/RI-BP86/def2-SV(P) is reported for this adduct in

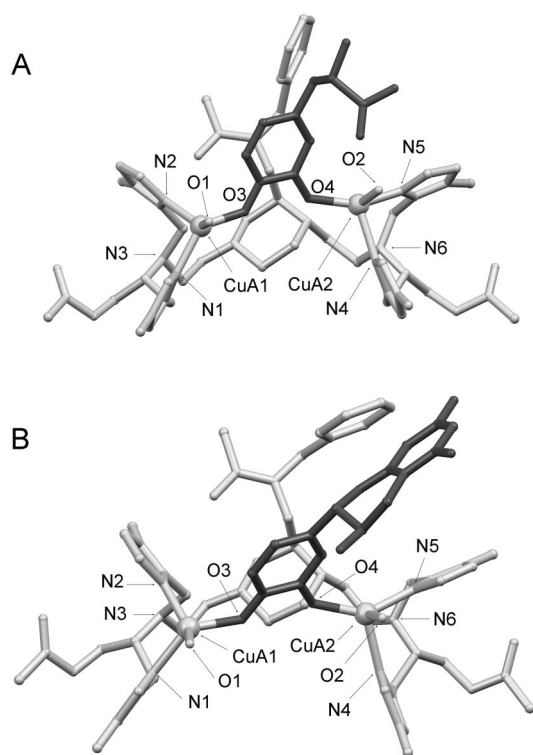


Fig. 9 (A) The optimized geometry (RI-BP86/def2-SV(P)) of the dinuclear copper complex with bound L-Dopa and (B) the optimized geometry (RI-BP86/def2-SV(P)) of the dinuclear copper complex with bound D-Catechin. Hydrogen atoms were not depicted in the structures for clarity. The L-Dopa and D-Catechin are drawn in dark grey and the complex backbone in light grey. Relevant calculated distances as depicted in (A): Cu(A1)–N1 = 2.087 Å, Cu(A1)–N2 = 2.094 Å, Cu(A1)–N3 = 4.383 Å, Cu(A1)–O1 = 1.900 Å, Cu(A1)–O3 = 1.975 Å, Cu(A2)–N4 = 2.306 Å, Cu(A2)–N5 = 2.048 Å, Cu(A2)–N6 = 3.667 Å, Cu(A2)–O2 = 1.945 Å, Cu(A2)–O4 = 1.928 Å. Relevant calculated distances as depicted in (B): Cu(A1)–N1 = 2.096 Å, Cu(A1)–N2 = 2.048 Å, Cu(A1)–N3 = 4.387 Å, Cu(A1)–O1 = 1.907 Å, Cu(A1)–O3 = 1.978 Å, Cu(A2)–N4 = 2.216 Å, Cu(A2)–N5 = 2.056 Å, Cu(A2)–N6 = 3.645 Å, Cu(A2)–O2 = 1.970 Å, Cu(A2)–O4 = 1.948 Å.

Fig. 9B. The weak interactions between bound substrate and the complex molecule involve here the chroman-3,5,7-triol residue, the phenylmethyl-*N*-acetoxy group and one *N*-methylimidazole unit located at the CuA2 site, all lying in close proximity to each other.

When the substrate binding to $[\text{Cu}_3(\text{L})]^{6+}$ is considered, probing the overall structural organization of the systems clearly becomes much more challenging. This is due to the presence of three Cu(II) centers, potentially catalytic, and to the fact that more possibilities of bridging interactions are now available. However, from the EPR analysis previously described, only two Cu(II) metal ions have been found to be catalytically active. We speculated that those centers were one CuA and the CuB, but without having direct knowledge of which one, CuA1 or CuA2, was actually the center involved in the redox process. We therefore tested several binding scenarios through a MMFF94/MC conformational search (Fig. 10). When L-Dopa binds to CuA1 and to the CuB site and in absence of a direct interaction of its amino acid portion with the remaining non-redox active copper center (Fig. 10A), the so obtained lowest energy conformer shows that chiral recognition should be very limited. In fact, none of the chiral residues of the complex can

significantly approach the chiral residue of the substrate. The same result is witnessed when the substrate binds to CuA2 and CuB, without further interaction with the CuA1 center (Fig. 10B). These conformations poorly explain the experimental results, since $[\text{Cu}_3(\text{L})]^{6+}$ shows the highest so far reported stereoselectivity of a model complex towards L-Dopa. When the substrate binds to the CuA1 and CuA2 sites as redox active centers, the CuB non-redox active site stays far away from the amino acid portion of the substrate (Fig. 10C), and so do the three chiral organic groups connected to the complex backbone. This conformational arrangement suggests that little chiral discrimination should be exerted, as in the binding scenario seen previously. Finally, as shown in Fig. 10D (L-Dopa binds to CuA1–CuB and interacts with CuA2) and Fig. 10E (L-Dopa binds to CuA2–CuB and interacts with CuA1), when an effective contact is present between the remaining redox innocent CuA center and the amino acid portion of L-Dopa, the recognition capability of the system seem to match both the catalysis results and the EPR findings. In line with this, the modest enantioselectivity exhibited by $[\text{Cu}_3(\text{L})]^{6+}$ in the catalytic oxidation of L-/D-DopaOMe and the other enantiomeric catechol derivatives, as anticipated earlier, could find their origin in the weaker anchoring ability of the amino acid portion of the substrates to one of the CuA centers not involved in the catalysis.

The lowest energy conformer obtained from the pool of substrate bound configurations screened above by MMFF94/MC, which corresponds to the structure depicted in Fig. 10E, was furthermore optimized without structural constraints by DFT/RI-BP86/def2-SV(P). The result is shown in Fig. 11 which highlights that the trinuclear copper complex can accommodate the L-Dopa substrate very well, and furthermore all three copper centers play an active although different role in substrate discrimination and catalysis.

When more bulky substrates such as L-/D-catechin are considered, the chiral discrimination featured by $[\text{Cu}_3(\text{L})]^{6+}$ decreases dramatically. Fig. 10F shows the lowest energy conformer (MMFF94/MC, substrate binds to the CuA2 and CuB sites) obtained by following the same procedures as described for L-Dopa. Whenever catechin binds to the complex, e.g. to the CuA2–CuA1 sites and/or to the CuA–CuB sites, in none of these binding scenarios can the –OH groups present in the chroman-3,5,7-triol residue productively approach the third (redox innocent) copper center as well as chiral regions of the ligand, which remain distant from the substrate. These structural aspects might explain the modest chiral recognition featured by $[\text{Cu}_3(\text{L})]^{6+}$ towards the flavonoids. From these modelling results, we may conclude that within the recognition process, the contribution brought by the two chiral *N*-(1-acetoxy-(*S*)-propyl) chains attached to the ligand scaffold should be very small in all cases. The folding effect of the third chiral center, namely the *N*-(phenylmethyl)-*N*-(acetoxy) chain connected to the piperazine residue, when the dinuclear copper complex is considered, the flexibility of the molecular backbone and the presence of a third copper ion in the trinuclear copper complex are, for this purpose, more relevant. The structural factors and their potential contribution to catalysis are difficult to dissect *a priori* since limited examples can be found in the literature for systems active towards biogenic catechols. Thus scarce guidelines exist that can be used and translated directly in the design process of synthetic functional systems which have performances comparable to those reported here. Nevertheless,

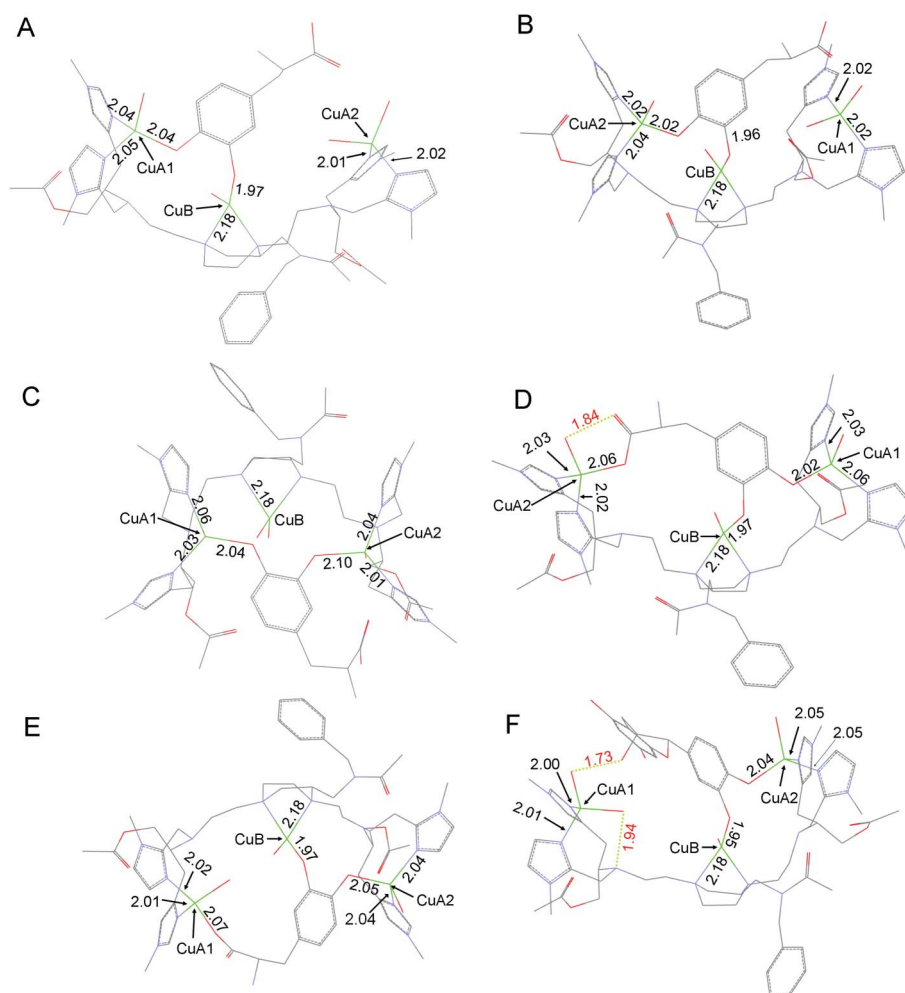


Fig. 10 The low energy conformers as obtained from MMFF94/MC conformational analyses showing the substrate–complex adducts in the case of the trinuclear copper complex $[\text{Cu}_3(\text{L})]^{6+}$. Hydrogen atoms have been omitted for clarity. (A) $[\text{Cu}_3(\text{L})\text{-L-Dopa}](\text{OH})_3$ (catechol binds to CuA1–CuB, heat of formation = $-1427.9 \text{ kJ mol}^{-1}$), (B) $[\text{Cu}_3(\text{L})\text{-L-Dopa}](\text{OH})_3$ (catechol binds to CuA2–CuB, heat of formation = $-1138.1 \text{ kJ mol}^{-1}$), (C) $[\text{Cu}_3(\text{L})\text{-L-Dopa}](\text{OH})_3$ (catechol binds to CuA1–CuA2, heat of formation = $-1135.9 \text{ kJ mol}^{-1}$), (D) $[\text{Cu}_3(\text{L})\text{-L-Dopa}](\text{OH})_3$ (catechol binds to CuA1–CuB and its amino acid residue interacts with CuA2, heat of formation = $-1213.6 \text{ kJ mol}^{-1}$), (E) $[\text{Cu}_3(\text{L})\text{-L-Dopa}](\text{OH})_3$ (catechol binds to CuA2–CuB and its amino acid residue interacts with CuA1, heat of formation = $-1111.2 \text{ kJ mol}^{-1}$), (F) $[\text{Cu}_3(\text{L})\text{-D-catechin}](\text{OH})_3$ (catechol binds to CuA2–CuB, heat of formation = $-1518.1 \text{ kJ mol}^{-1}$). The heat of formation for these systems were calculated by single point semi-empirical PM3tm method, in the high spin configurations ($S = 3/2$).

we note that besides the clear limits towards direct applications, it is possible to further improve the recognition capacity of these complexes by additional modification of the chiral ligand, *e.g.* by adding chiral functionalities much closer to the nitrogen donors in the imidazole rings. In addition there is an enormous possibility to elaborate the identity of the trinuclear complex reported in this work by replacing the Cu^{II} ions with different metal ions. In this way, trinuclear mixed-metal complexes with appropriate characteristics to promote specific catalytic reactions could be obtained.

Conclusions

In this work we described a new poly-imidazole N_3 -ligand, $[(S)\text{-Pz-(C2-(HisIm))}_2]$, which combines three chiral centers with (*S*) configuration and three coordination sites for metal complexation in the organic scaffold. The dinuclear and trinuclear copper(II)

complexes derived from $[(S)\text{-Pz-(C2-(HisIm))}_2]$ show large conformational flexibility, due to the poor coordination ability of the tertiary amino groups located in the ligand side-chains containing the imidazole units, and this feature favors the interaction with substrate molecules in the catalytic reactions. The structure and electronic characteristics of the metal centers were probed theoretically (DFT/RI-PB86/TZVP) and experimentally by low-temperature EPR analysis. Both the $[\text{Cu}_2(\text{L})]^{4+}$ and $[\text{Cu}_3(\text{L})]^{6+}$ complexes perform stereoselective oxidations of optically active catechol and flavonoid compounds. For $[\text{Cu}_2(\text{L})]^{4+}$, chiral recognition of the substrates is driven by electrostatic interactions between the bound substrate and folded regions of the coordinated ligand. The same effects, although much less prominent, should rule the recognition mechanism of $[\text{Cu}_3(\text{L})]^{6+}$ towards bulky substrates. For $[\text{Cu}_3(\text{L})]^{6+}$ on the other hand, the strong recognition towards L/D-Dopa must be associated with the direct participation of the non-catalytic copper center in the interaction with the substrate.

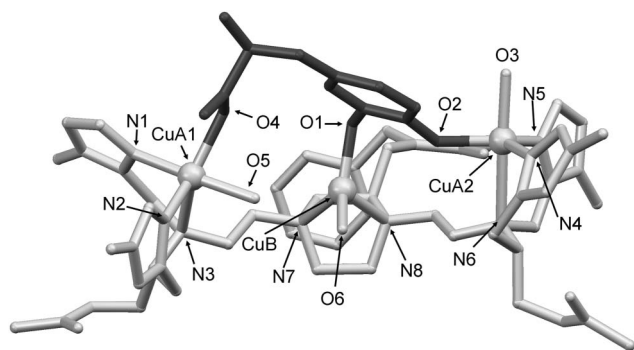


Fig. 11 The optimized geometry (RI-BP86/def2-SV(P)) of the neutral adduct $[\text{Cu}_3(\text{L})\text{-L-Dopa}](\text{OH})_3$ with catechol binding to CuA2–CuB sites and amino acid portion of the substrate interacting with CuA1. Hydrogen atoms were not depicted in the structure for clarity. The L-Dopa is drawn in dark grey and the complex backbone in light grey. Relevant calculated distances: Cu(A1)–N1 = 2.025 Å, Cu(A1)–N2 = 2.048 Å, Cu(A1)–N3 = 2.511 Å, Cu(A1)–O4 = 2.118 Å, Cu(A1)–O5 = 2.084 Å, Cu(A2)–N4 = 1.943 Å, Cu(A2)–N5 = 1.937 Å, Cu(A2)–N6 = 2.532 Å, Cu(A2)–O2 = 1.911 Å, Cu(A2)–O3 = 1.967 Å, CuB–N7 = 2.190 Å, CuB–N8 = 2.180 Å, CuB–O1 = 1.957 Å, CuB–O6 = 1.947 Å.

Further work aimed at extending the scope of the catalytic reactions and chiral discrimination by the trinuclear complexes towards different types of polyfunctional substrate molecules are currently on the way.

Experimental

Materials and methods

Compounds and solvents accessible from commercial sources were of the highest purity available and used as received. Acetonitrile (spectral grade) was distilled from potassium permanganate and from sodium carbonate; it was then stored over calcium hydride and distilled before use under an inert atmosphere (UV cut-off <190 nm). Tetrahydrofuran (THF) was dried by refluxing and distilling from metallic sodium. Dimethylformamide (DMF) was purified by treatment with barium oxide and distilled over calcium hydride under reduced pressure. Anhydrous methanol was obtained with activated 3 Å molecular sieves. Elemental analyses were performed at the microanalytical laboratory of the Inorganic Chemistry Department in Milan with a Perkin Elmer 2400 Analyzer. Optical rotations were obtained from a Perkin–Elmer 241 polarimeter at 25 °C using a quartz cell of 10 cm path length. Mass spectra (MS) were obtained using a Thermo-Finnigan LCQ Advantage electrospray ionization (ESI) mass spectrometer. UV-vis spectra were recorded on HP 8452A or HP 8453 diode array spectrophotometers equipped with a magnetically stirred, thermostated cell holder maintained at 20 ± 0.1 °C. Circular dichroism (CD) spectra were recorded with a Jasco J-500 spectropolarimeter using quartz cells of 0.1–2.0 cm path length. ^1H NMR, ^{13}C NMR spectra were recorded with a Bruker AVANCE 400 spectrometer operating at 9.37 T. Atomic absorption measurements were performed with a Perkin–Elmer 3100 AAS spectrometer. ICP measurements were obtained using a Thermo-Jarrel Ash ThermoElemental IRIS INTREPID.

Azide binding measurements. The binding of azide to $[\text{Cu}_2(\text{L})][\text{ClO}_4]_4 \cdot 4\text{H}_2\text{O}$ and $[\text{Cu}_3(\text{L})][\text{ClO}_4]_6 \cdot 6\text{H}_2\text{O}$ was studied spec-

trophotometrically by adding concentrated methanolic solutions of sodium azide to solutions of the complexes dissolved in the MeOH–MeCN 9 : 1 (v/v). All measurements were performed in a thermostated optical cell, with magnetic stirring, at 20 ± 0.1 °C. In all cases, it was found that binding of the anion is fast, so that no incubation of the mixtures was necessary before the spectroscopic measurements. Titration of $[\text{Cu}_2(\text{L})]^{4+}$ ($2.19 \times 10^{-4} \text{ dm}^3 \text{ mol}^{-1} \text{ cm}^{-1}$) was performed by stepwise addition of 0.1 molar equiv. azide (from a $1.01 \times 10^{-3} \text{ dm}^3 \text{ mol}^{-1} \text{ cm}^{-1}$ solution), up to 2.0 [azide] : $[\text{Cu}_2]$ molar ratio. Further addition of azide did not produce appreciable spectral changes. It was possible to separate the titration steps for $[\text{N}_3^-] : [\text{Cu}_2]$ between 0.1 and 1.0 ($\lambda_{\text{max}} = 412 \text{ nm}$, isosbestic point at 350 nm) and between 1.1 to 2.0 ($\lambda_{\text{max}} = 412 \text{ nm}$, isosbestic point at 346 nm). In a similar way, titration of $[\text{Cu}_3(\text{L})]^{6+}$ ($2.93 \times 10^{-4} \text{ dm}^3 \text{ mol}^{-1} \text{ cm}^{-1}$) was carried out by stepwise addition of 0.1 molar equiv. of azide (from a $1.01 \times 10^{-3} \text{ dm}^3 \text{ mol}^{-1} \text{ cm}^{-1}$ solution) between 0.1 to 2.0 $[\text{N}_3^-] : [\text{Cu}_3]$ ratios, and then 0.2 molar equiv. of azide from 2.2 to 4.0 $[\text{N}_3^-] : [\text{Cu}_3]$ ratios. In this case, it was not possible to separate the various steps of the titration. To determine the binding constants and stoichiometry of formation of the adducts formed by $[\text{Cu}_2(\text{L})]^{4+}$, the spectral data were analyzed as previously described.⁶⁷

EPR measurements and data analysis. The low temperature EPR spectra were acquired with an X-band (9.57 GHz) cavity on a Bruker EleXsyS 560 Super X spectrometer by using a liquid nitrogen bath-finger for the $T = 77 \text{ K}$ experiments or by employing the (100–600 K) ER4131VT EPR-ENDOR variable temperature control unit, for the temperature experiments at $T = 120 \text{ K}$. The cryogenic measurements were performed with a dual-band X-resonator (Bruker dm9511) and by using a He-flow cryostat (ESR 900, Oxford Instruments). The freshly prepared solutions for the exogenous ligand-free complexes and azide adducts were degassed by exchange with argon prior to measurements. The reactions between L-Dopa and the dinuclear and trinuclear Cu complexes were carried out under rigorous anaerobic conditions by fast mixing equimolar amounts of the complexes (in MeCN–MeOH) containing a twofold excess of 3-methyl-2-benzothiazolinone hydrazone and the substrate (in MeOH) kept in air-tight syringes directly into quartz EPR tubes, which were maintained under argon and sealed by using a rubber septum. The reaction mixtures (copper complexes + MBTH + L-Dopa) were quenched after few seconds by fast-freezing the EPR tubes with liquid nitrogen. The same quartz EPR tubes were used after the low temperature measurements as UV/vis cells to control the optical properties (at r.t.) of the reacted samples. The pH dependent EPR traces were recorded by dissolving the powdered complexes in a mixture of aqueous phosphate buffer (50 mM, from pH 8.6 to pH 5.5) and methanol (9 : 1, v/v). All the EPR spectra were baseline corrected upon subtraction of both the cavity background and the EPR tube containing the solvent (MeOH–MeCN), keeping the same filling volume. Care was taken to avoid microwave signal saturation within acquisition. The WinSimFonia simulation program working at the second-order perturbation theory (ver. 1.25) and WinEPR (ver. 2.11) software were provided by Bruker. Cu–EDTA standard solution (1 mM MeOH–MeCN, 8 : 2, v/v) was used to estimate the samples' spin concentration, by comparing the double integrated signal intensity of the samples with that of the standard under

identical experimental conditions (temperature, gain, sweep time, modulation amplitude, and microwave power).

Theoretical modelling of the copper(II) complexes. The structure and electronic characteristics (in the gas phase) of the dinuclear and trinuclear Cu complexes were investigated by quantum-chemical methods. To this end, the structures of the species charged $[\text{Cu}_2(\text{L})(\text{H}_2\text{O})_4]^{4+}$, neutral $[\text{Cu}_2(\text{L})(\text{OH})_4]$, charged $[\text{Cu}_3(\text{L})(\text{H}_2\text{O})_6]^{6+}$ and neutral $[\text{Cu}_3(\text{L})(\text{OH})_6]$ were optimized, introducing water molecules or for the neutral forms hydroxide ions (OH^-) instead of perchlorates (ClO_4^-) as negative ligands for the cationic Cu clusters since we were interested in modelling the species active in the catalysis (MeOH–PBS buffer, pH = 8.6), *i.e.* in solution, where solvent molecules ($\text{H}_2\text{O}/\text{OH}^-$) are the ligands filling the coordination sphere of the metal ions. In the most simplified picture, each cluster is composed by the two Cu–imidazole plus tertiary amino coordinated units (CuA sites) linked together through the piperazine spacer, which contains the *N*-donors for the third copper site (namely CuB) in the trinuclear cluster. A pre-screening among the possible conformational arrangements of the copper coordination sites and the molecular linker was performed by using a combination of Merck Molecular Mechanics Force Field (MMFF94)/Monte Carlo methods, which employs simulated “annealing” to generate conformations of the molecule followed by geometry optimization with the semiempirical PM3tm method as implemented in the computational package Spartan 08.⁹² It was observed that, in order to reduce the steric hindrance and optimize the copper-donor (N,O) interactions, the linker adopts a chair-conformation in the dinuclear cluster and the boat conformation in the trinuclear complex. The two CuA halves and the CuB site were therefore optimized separately; in order to reduce the computational cost, the DFT optimizations were performed by using the BP86 functional,^{93–97} (m3-grid) in combination with the Resolution of Identity (RI-BP86) technique, as it is implemented in the TURBOMOLE V5.10 package.^{98–102} The basis set used was the def2-TZVP.^{98–101} The obtained units were finally assembled (with the piperazine in the correct conformation) and the resulting di- and trinuclear clusters were finally optimized at RI-BP86 level, by using the TZVP basis set.⁹⁸ For the trinuclear cluster, SCF convergence problems were solved by imposing a strong damping during the first SCF iterations; the SCF convergence threshold was 10^{-5} a.u. Geometry optimizations were converged within the thresholds of 10^{-6} a.u. for the change in energy and 10^{-3} a.u. for the maximum of the gradient norm. Due to the high conformational freedom, many local minima were found in both di- and trinuclear clusters, corresponding to a relative rotation of the two halves along the ethyl axis. Among the different conformations, the most stable were taken; in particular the chosen ones are lower in energy by 20.5 kJ mol⁻¹ and 157.3 kJ mol⁻¹, as compared to the other conformers, for the di- and trinuclear clusters, respectively. The relative stability of the electronic states due to ferro- and antiferro-magnetic coupling, in the trinuclear neutral cluster was obtained using the broken-symmetry spin-flip approach,¹⁰² as it is implemented within the TURBOMOLE V5.10 software package. In order to explore the molecular conformations adopted by $[\text{Cu}_2(\text{L})]^{4+}$ and $[\text{Cu}_3(\text{L})]^{6+}$ upon substrate binding, the molecular modelling was carried out in a vacuum starting from the neutral forms (with OH^- counter-anions) using combination of Monte Carlo/MMFF94,¹⁰³ which includes parameterizations

for the $\text{Cu}^{2+}/\text{Cu}^+$ pair (copper VDW radius = 0.15723 nm), as implemented in Spartan 08.⁹² Constraints have been applied only in the case of the trinuclear copper complex (the CuB–N distances were kept frozen at 2.18 Å). It is important to notice that the conformational space to be explored is very large, due to the presence of several σ -bonds in the metal–organic backbone and therefore a complete exploration (systematic search) is computationally unfeasible. However by starting the MC search from different initial conformations the results yielded similar lowest energy conformers. The initial temperature for the Monte Carlo (MC)/Simulated-Annealing algorithm was set to $T = 5000$ K. Restricted searches were applied, using an energy window of $E_{\text{max}} = 40$ kJ mol⁻¹ from a setting pool of maximum 10^4 conformers. The lowest energy conformers were selected and screened by single-point energy calculations (SP) using the semiempirical PM3tm method. Only neutral forms and high-spin structures ($S = 1$ for the dinuclear copper–substrate adducts and the $S = 3/2$ for the trinuclear copper–substrate adducts) were considered. Some of the lowest energy conformers were chosen, namely $[\text{Cu}_2(\text{L})\text{-L-Dopa}](\text{OH})_2$, $[\text{Cu}_2(\text{L})\text{-D-catechin}](\text{OH})_2$ and $[\text{Cu}_3(\text{L})\text{-L-Dopa}](\text{OH})_3$, and optimized further without any constraints through quantum-chemical methods using DFT/RI-BP86/def2-SV(P) with the same threshold for energies and gradients as achieved for the substrate-free complexes previously reported. The TURBOMOLE calculations were performed on the STALLO, Cluster Platform HP 3000 BL460c computer facility, NOTUR, Norway.

Catalytic oxidation of *o*-catechols and flavonoids. The kinetics of catalytic oxidation of the *o*-diphenols L-Dopa, D-Dopa, L-DopaOMe, D-DopaOMe, L-norepinephrine, and D-norepinephrine were studied by UV-vis spectroscopy using a magnetically stirred and thermostated 1 cm path length cell. The temperature during the measurements was kept constant at 20 ± 0.1 °C. A mixture of aqueous phosphate buffer (50 mM, pH 8.6) and methanol (9:1, v/v) saturated with atmospheric oxygen was used as solvent. The experiments were carried out over a substrate concentration range and were initiated by adding a few microliters of solutions of the complexes (final concentrations 3.45×10^{-6} dm³ mol⁻¹ cm⁻¹ for $[\text{Cu}_2(\text{L})][\text{ClO}_4]_4 \cdot 4\text{H}_2\text{O}$ and 3.15×10^{-6} dm³ mol⁻¹ cm⁻¹ for $[\text{Cu}_3(\text{L})][\text{ClO}_4]_6 \cdot 6\text{H}_2\text{O}$) in all the experiments, while the substrate concentration was varied from 4.0×10^{-6} dm³ mol⁻¹ cm⁻¹ to 1.0×10^{-3} dm³ mol⁻¹ cm⁻¹ (final volume 2 cm³). To prevent further reactions of the quinones initially formed, an excess amount of 3-methyl-2-benzothiazolinone hydrazone (MBTH, 1.0×10^{-3} dm³ mol⁻¹ cm⁻¹) was added. The formation of the corresponding stable *ortho*-quinones–MBTH adducts was followed through the development of the strong absorption band at 500 nm for L-/D-Dopa and their methyl esters ($\epsilon_{500} = 13\,400$ dm³ mol⁻¹ cm⁻¹ for Dopa-*ortho*-quinone–MBTH, and $\epsilon_{500} = 11\,600$ dm³ mol⁻¹ cm⁻¹ for DopaOMe-*ortho*-quinone–MBTH, respectively), and at 511 nm for L-/D-norepinephrine ($\epsilon_{511} = 4835$ dm³ mol⁻¹ cm⁻¹ for norepinephrine-*ortho*-quinone–MBTH). The catalytic oxidations of the flavonoids L-epicatechin and D-catechin were studied by UV-vis spectroscopy, using a mixture of aqueous phosphate buffer (50 mM, pH 7.0)–methanol (9:1, v/v) saturated with atmospheric oxygen, as solvent. The experiments were carried out as reported above for the other substrates and, in this case, MBTH was also added (1.0×10^{-3} dm³ mol⁻¹ cm⁻¹)

to prevent further reactions of the quinones initially formed. The formation of the stable quinone–MBTH adducts was followed through the development of the strong absorption band at 463 nm ($\epsilon_{463} = 18950 \text{ dm}^3 \text{ mol}^{-1} \text{ cm}^{-1}$) for L-epicatechin-quinone–MBTH and at 459 nm ($\epsilon_{459} = 17230 \text{ dm}^3 \text{ mol}^{-1} \text{ cm}^{-1}$) for D-catechin-quinone–MBTH, respectively.⁶⁵ In all the experiments, the noise was reduced by reading the absorbance difference between the λ_{max} of the adducts and that at 900 nm, and the initial rates of oxidation were obtained by fitting the absorbance *versus* time curves in the first few seconds of the reactions. The dependence of the rates of the catalytic reactions as a function of the substrate concentration exhibited a general hyperbolic behavior; therefore the kinetic parameters (k_{cat} , K_{M}) were estimated by fitting the data using the Michaelis–Menten equation, implemented in the FigSys® software. Nevertheless, a substrate (S) inhibition effect was detected in the oxidation of L-epicatechin and D-catechin with $[\text{Cu}_2(\text{L})]^{4+}$ and in the oxidation of L-DopaOMe, D-DopaOMe, L-epicatechin and D-catechin with $[\text{Cu}_3(\text{L})]^{6+}$, and therefore the reaction rates did not reach a plateau at high substrate concentrations. This behavior can be explained by considering that, in the presence of a large excess of substrate, coordination of two molecules of substrate to the complex occurs, each one chelating the reactive CuA centers. The bis-catecholato adduct is catalytically inert and prevents the formation of a bridged catecholato adduct, which is the reactive intermediate that generates the *ortho*-quinone. Hence, in the presence of substrate inhibition effect, the kinetic parameters (k_{cat} , K_{M}) were estimated by fitting the rate data with the following kinetic equation, where K_{C} is the catechol binding constant for the bis-adduct (inhibition constant) and K_{M} is the constant for the bridge catecholato adduct (productive binding):

$$V = \frac{k_{\text{cat}} [\text{S}]}{K_{\text{M}} (1 + K_{\text{C}} [\text{S}]^2) + [\text{S}]} \quad (3)$$

The degree of stereoselectivity in the catalytic reactions by the dinuclear and trinuclear copper complexes was evaluated through the use of eqn (4):

$$\text{R\%} = \frac{\left[\left(\frac{k_{\text{cat}}}{K_{\text{M}}} \right)_{\text{D}} - \left(\frac{k_{\text{cat}}}{K_{\text{M}}} \right)_{\text{L}} \right]}{\left[\left(\frac{k_{\text{cat}}}{K_{\text{M}}} \right)_{\text{D}} + \left(\frac{k_{\text{cat}}}{K_{\text{M}}} \right)_{\text{L}} \right]} \times 100 \quad (4)$$

where k_{cat} and K_{M} represent the turnover rate constant and substrate binding affinity constant, respectively.

Synthesis of (S)-Pz-(C2-(HisIm))₂ (L). The ligand, (S)-2-piperazinemethanamine, 1,4-bis[2-((N-(1-acetoxy-3-(1-methyl-1H-imidazol-4-yl))-2-(S)-propyl)-(N-(1-methyl-1H-imidazol-2-ylmethyl)))ethyl]-N-(phenylmethyl)-N-(acetoxy)-, also named (S)-Pz-(C2-(HisIm))₂ (L), was prepared following this synthetic route.

(S)-1,4-Bis(tert-butoxycarbonyl)piperazine-2-carboxylic acid, (2). (S)-Piperazine carboxylic acid hydrochloride **1** (1.00 g, 4.94 mmol) was suspended in a mixture of water and dioxane (30 cm³; 1:1, v/v) and KOH (1.4 g, 24.7 mmol) was added until the amino acid hydrochloride was completely dissolved. Then, di-*tert*-butylcarbonate (Boc, 3.23 g, 14.8 mmol) was poured into the solution and KOH was added again to obtain an alkaline pH. The mixture was stirred vigorously overnight at room temperature, the solvent was evaporated, and the white solid residue was treated with water (50 cm³) and extracted with

ethyl acetate (2 × 30 cm³) to remove by-products. Afterwards, the pH of the aqueous phase was adjusted to 2–3 with KHSO₄, observing strong foaming and formation of a white precipitate. The solution was extracted first with ethyl acetate (1 × 40 cm³) and then with dichloromethane (2 × 40 cm³). The combined organic phases were dried with anhydrous Na₂SO₄ and, after filtration, the solvent was removed yielding a pasty, spongy, white crude product (1.64 g), which was recrystallized with benzene–*n*-hexane. White crystals (1.26 g, 77.4%) of the pure product were obtained. $[\alpha]_{\text{D}}^{22}$ ($T = 293 \text{ K}$) = -14.39 ($c = 7.57 \times 10^{-3} \text{ M}$ in CHCl₃). Found: C, 54.65; H, 7.96; N, 8.45; M⁺, 331. C₁₅H₂₆N₂O₆ requires: C, 54.53; H, 7.93; N, 8.48; M, 330.18. UV-vis λ_{max} (CH₃CN)/nm 202 ($\epsilon/\text{dm}^3 \text{ mol}^{-1} \text{ cm}^{-1}$ 600), 206 (750), 209 (800), 225 (2850), 238 (110). CD λ_{max} (CH₃CN)/nm; 207sh ($\Delta\epsilon/\text{dm}^3 \text{ mol}^{-1} \text{ cm}^{-1}$ +0.3), 215sh (+0.8), 222 (+1.0), 248 (−0.1). ¹H NMR (400 MHz; CDCl₃; Me₄Si; 298 K): δ (ppm) = 1.43 (s, 18H, CH₃), 2.85 (dd, 1H, ²*J* = 13.2 Hz, CH₂), 3.10 (dd, 1H, ²*J* = 12.8 Hz, ³*J* = 2.4 Hz, CH₂), 3.21 (dd, 1H, ²*J* = 11.2 Hz, CH₂), 3.81 (dd, 1H, CH₂), 3.98 (dd, 1H, CH₂), 4.54 (dd, 1H, CH₂), 4.57 (s, 1H, CH). ¹³C NMR (100.6 MHz, CDCl₃, 298 K): δ (ppm) 28.3, 40.2, 42.9, 44.6, 53.5, 80.9, 154.5, 174.4

(S)-1,4-Piperazinedicarboxylic acid, 2-[(phenylmethyl)-amino]carbonyl-1,4-bis(*tert*-butyl) ester (3). The protected compound **2** (1.24 g, 3.75 mmol) was rapidly dissolved in DMF (20 cm³) and HBTU (*o*-(benzotriazol-1-yl)-*N,N,N',N'*-tetramethyluronium hexafluorophosphate, 2.84 g, 7.49 mmol) was poured into the solution. Benzylamine (802 mg, 7.49 mmol) was added dropwise as a solution in DMF (1:4, v/v) and finally triethylamine (2.61 cm³, 18.7 mmol) was added as a base. The reaction mixture was stirred vigorously for 3 days at room temperature under an inert atmosphere. Then, the solvent was evaporated, yielding a highly viscous yellowish oil. This was treated with a saturated aqueous solution of NaHCO₃ (100 cm³) and extracted with dichloromethane (3 × 70 cm³). The organic phase was washed with a saturated aqueous solution of KHSO₄ (1 × 150 cm³) and then with brine (1 × 150 cm³). Removal of the solvent gave a yellow oil, which was purified by silica flash chromatography (3 × 15 cm) following these conditions: pressure 2 in min^{−1}, eluent petroleum ether–ethyl acetate (from 7:3 to 1:1, v/v). A white solid (1.40 g, 89%) was obtained. $[\alpha]_{\text{D}}^{22}$ ($T = 293 \text{ K}$) = -20.79 ($c = 9.06 \times 10^{-3} \text{ M}$ in CHCl₃). Found: C, 62.90; H, 8.01; N, 9.96; M⁺, 420. C₂₂H₃₃N₃O₅ requires C, 62.99; H, 7.93; N, 10.02; M, 419.5. UV-vis λ_{max} (CH₃CN)/nm 203sh ($\epsilon/\text{dm}^3 \text{ mol}^{-1} \text{ cm}^{-1}$ 600), 210sh (680), 226sh (2450), 241 (450), 253 (250), 259 (250), 265sh (190), 268sh (140). CD λ_{max} (CH₃CN)/nm 207 ($\Delta\epsilon/\text{dm}^3 \text{ mol}^{-1} \text{ cm}^{-1}$ −2.0), 224sh (−1.1), 229 (−1.2), 240sh (−0.6). ¹H NMR (400 MHz, CDCl₃, Me₄Si, 298 K): δ (ppm) 1.45 (s, 18H, CH₃), 3.00 (m, 1H, CH₂), 3.14 (m, 1H, CH₂), 3.18 (dd, 1H, ²*J* = 13.6 Hz, ³*J* = 4.4 Hz, CH₂), 3.87 (m, 1H, CH₂), 3.87 (m, 1H, CH₂), 4.46 (dd, 1H, CH₂), 4.46 (s, 2H, CH₂), 4.62 (m, 1H, CH), 6.46 (s, 1H, NH), 7.24–7.34 (m, 5H, CH-phenyl). ¹³C NMR (100.6 MHz, CDCl₃, 298 K): δ (ppm) 28.2, 43.6, 53.6, 80.3, 127.4, 127.5, 128.6, 138.0, 154.6, 169.1.

(S)-2-Piperazinecarboxamide,1,4-bis(trifluoroacetate)-N-(phenylmethyl) (4). To remove the Boc groups, a solution of dichloromethane and trifluoroacetic acid (40 mL, 1:1, v/v) previously cooled to 4 °C was poured onto compound **3** (1.35 g, 3.2 mmol) in a round-bottomed flask. The mixture was stirred at

room temperature for 2 h. Finally, the solvent was removed by rotary evaporation and dried under vacuum, affording a yellow solid in quantitative yield (1.43 g). $[\alpha]_D^{22}$ ($T = 293$ K) = +11.62 ($c = 8.85 \times 10^{-3}$ M in CH_3OH). Found C, 42.90; H, 4.25; N, 9.30; M^+ , 448. $\text{C}_{16}\text{H}_{19}\text{F}_6\text{N}_3\text{O}_5$ requires C, 42.96; H, 4.28; N, 9.39; M , 447.3. UV-vis 204sh ($\epsilon/\text{dm}^3 \text{ mol}^{-1} \text{ cm}^{-1}$ 2700), 208sh (2370), 216 (2 625), 248sh (130), 252 (165), 258 (200), 264sh (150). CD $\lambda_{\text{max}}(\text{CH}_3\text{OH})/\text{nm}$ 207 ($\Delta\epsilon/\text{dm}^3 \text{ mol}^{-1} \text{ cm}^{-1}$ -2.1), 223sh (-1.1), 228 (-1.2), 240sh (-0.7). ^1H NMR (400 MHz, CD_3OD , Me_4Si , 298 K): δ (ppm) 3.45 (dd, 1H, $^2J = 13.6$ Hz, $^3J = 3.6$ Hz, CH_2), 3.53 (dd, 1H, $^2J = 14.0$ Hz, $^3J = 3.6$ Hz, CH_2), 3.58 (dd, 1H, $^2J = 13.6$ Hz, CH_2), 3.77 (dd, 1H, CH_2), 3.86 (dd, 1H, CH_2), 3.97 (dd, 1H, CH_2), 4.48 (s, 2H, CH_2), 4.50 (dd, 1H, CH), 7.35–7.47 (m, 5H, CH-phenyl). ^{13}C NMR (100.6 MHz, CD_3OD , 298 K): δ (ppm) 39.6, 39.8, 42.5, 43.6, 53.6, 127.5, 127.9, 129.0, 137.0, 164.3.

(S)-2-Piperazinecarboxamide,1,4-bis(2-chloroacetyl)-N-(phenylmethyl), (5). Compound **4** (654 mg, 1.47 mmol) was suspended in anhydrous dichloromethane in a round bottomed flask (40 cm^3) and gaseous ammonia was bubbled into the suspension for 0.5 h, while cooling with an ice bath. Then, the organic solution was filtered off and the solid residue was treated again twice in the same manner. The organic phases were combined and the solvent was evaporated, yielding oil which was dried under high vacuum. The free amino intermediate so obtained was subjected to a condensation under Groszkowski conditions.¹⁰⁴ The resulting oil was dissolved in anhydrous chloroform (30 cm^3) and the solution was cooled to 5 °C under vigorous stirring. Then, dry Na_2CO_3 (775 mg, 7.31 mmol) was poured into the solution and chloroacetyl chloride (280 μl , 3.51 mmol), diluted in anhydrous chloroform (2–3 cm^3), was added dropwise. The reaction was allowed to proceed for 2 h, keeping the temperature between 5 °C and 8 °C, and later overnight at room temperature under inert atmosphere. The reaction was checked by TLC (dichloromethane–methanol, 9:1, v/v), and a mixture (roughly 1:1) of the desired diacetylated product ($R_f = 0.6$) and of the monoacetylated amine ($R_f = 0.3$) was obtained, with traces of the unreacted diamine starting material. Thus, a further aliquot of chloroacetyl chloride (280 μl , 3.51 mmol) was added dropwise to the solution at 5 °C and the reaction was allowed to continue for a further 24 h. TLC analysis showed that all the reagent was completely converted into the diacetylated product, which was purified by silica flash chromatography (3 \times 15 cm) following these conditions: pressure 1 in min^{-1} , eluent dichloromethane–methanol (100:0–95:5, v/v). A white solid (535 mg, >97%) was obtained. $[\alpha]_D$ ($T = 293$ K) = -63.01 ($c = 9.72 \times 10^{-3}$ M, CHCl_3). Found: C, 51.73; H, 5.11; N, 11.36; M^+ , 372. $\text{C}_{16}\text{H}_{19}\text{Cl}_2\text{N}_3\text{O}_3$ requires C, 51.62; H, 5.14; N, 11.29; M , 371.1. UV-vis $\lambda_{\text{max}}(\text{CH}_3\text{CN})/\text{nm}$ 201 ($\epsilon/\text{dm}^3 \text{ mol}^{-1} \text{ cm}^{-1}$ 3 340), 205 (3 740), 213 (4 040), 219sh (9 500), 227 (6 100), 262sh (550). CD $\lambda_{\text{max}}(\text{CH}_3\text{CN})/\text{nm}$ 209 ($\Delta\epsilon/\text{dm}^3 \text{ mol}^{-1} \text{ cm}^{-1}$ -2.2), 219sh (-4.0), 228 (-5.1), 257 (+0.3). ^1H NMR (400 MHz, CDCl_3 , Me_4Si 298 K) δ (ppm) 2.85 (m, 1H, $^2J = 13.6$ Hz, CH_2), 3.30 (m, 1H, $^2J = 14.0$ Hz, CH_2), 3.77 (m, 1H, CH_2), 4.07 (s, 4H, CH_2), 4.22 (m, 1H, $^2J = 13.2$ Hz, CH_2), 4.40 (d, 2H, $^3J = 5.6$ Hz, CH_2), 4.53 (m, 1H, CH_2), 4.58 (m, 1H, CH_2), 5.16 (m, 1H, CH), 6.73 (s, broad, 1H, NH), 7.19–7.34 (m, 5H, CH-phenyl). ^{13}C NMR (100.6 MHz, CDCl_3 , 298 K): δ (ppm) 40.6, 41.2, 41.9, 43.7, 43.9, 45.1, 52.6, 127.4, 127.6, 128.6, 128.7, 137.4, 167.4, 167.8, 168.8.

(S)-2-Piperazinecarboxamide,1,4-bis[2-(N-(1-(S)-methoxycarbonyl-2-(1-methyl-1H-imidazol-4-yl))-1-acetyl)-N-(phenylmethyl), (6). All the following steps were performed with carefully dried solvents and under an inert atmosphere. *N*-Methylhistidine methyl ester dihydrochloride, prepared according to Noordam's method,¹⁰⁵ (2.76 g, 10.77 mmol) was suspended in anhydrous dichloromethane (150 cm^3) in a round-bottomed flask. The mixture was cooled with an ice bath and gaseous ammonia was bubbled for 0.5 h. The liquid was filtered off and the solid residue was treated again twice following the same procedure. The organic phases were collected and the solvent was evaporated, affording an orange oil of the free amino ester. This was then dissolved in *N*-methyl pyrrolidone (40 cm^3) and a solution of compound **5** (1.60 g, 4.31 mmol) was added. After few min, triethylamine (6 cm^3 , 43.1 mmol) was added dropwise into the solution. The solution was kept to 80 °C overnight. The reaction was followed by TLC (dichloromethane–methanol–ammonia, 9:1:0.1, v/v/v), showing the formation of a new product ($R_f = 0.25$). Further analysis on the crude mixture by ESI-MS demonstrated this to be the desired condensed product. The solvent was evaporated and the oily, crude dark brown product was purified by silica flash chromatography (3 \times 15 cm) following these conditions: pressure 1 in min^{-1} , eluent dichloromethane–methanol–ammonia (94:6:10–70:30:10, v/v/v). Orange oil (1.09 g, 38%) was obtained. $[\alpha]_D^{22}$ ($T = 293$ K) = -31.24 ($c = 6.01 \times 10^{-3}$ M in CHCl_3). Found: C, 57.51; H, 6.61; N, 18.83; M^+ , 666. $\text{C}_{32}\text{H}_{43}\text{N}_9\text{O}_7$ requires C, 57.73; H, 6.51; N, 18.94; M , 665.7. UV-vis $\lambda_{\text{max}}(\text{CH}_3\text{CN})/\text{nm}$ 202 ($\epsilon/\text{dm}^3 \text{ mol}^{-1} \text{ cm}^{-1}$ 4890), 207 (5520), 219 (15 980), 238sh (4490), 249sh (1430), 312 (830), 325sh (730), 356sh (290). CD $\lambda_{\text{max}}(\text{CH}_3\text{CN})/\text{nm}$ 208 ($\Delta\epsilon/\text{dm}^3 \text{ mol}^{-1} \text{ cm}^{-1}$ -4.9), 218 (+0.1), 230 (-2.1), 237sh (-1.6), 249sh (-0.5). ^1H NMR (400 MHz, CDCl_3 , Me_4Si , 298 K): δ (ppm) 2.50–3.50 (m, 10H, CH_2), 3.57 (s, 4H, CH_2), 3.61 (s, 6H, CH_3), 3.70 (m, 2H, CH), 3.70 (s, 6H, CH_3), 4.39 (d, 2H, $^3J = 5.6$ Hz, CH_2), 5.13 (m, 1H, CH), 5.13 (s, 1H, NH-amino), 5.53 (s, 1H, NH-amino), 6.45 (s, 2H, CH), 6.65 (d, 1H, $^3J = 5.6$ Hz, NH-amide), 7.16–7.30 (m, 5H, CH-phenyl), 7.31 (s, 2H, CH). ^{13}C NMR (100.6 MHz, CDCl_3 , 298 K): δ (ppm) 31.5, 33.2, 40.9, 43.4, 48.7, 49.2, 50.8, 51.7, 51.9, 60.8, 61.2, 117.7, 127.2, 127.4, 128.5, 137.4, 138.2, 138.3, 170.1, 171.2, 173.2, 174.2, 174.7.

(S)-2-Piperazinecarboxamide,1,4-bis[2-((N-(1-(S)-methoxycarbonyl-2-(1-methyl-1H-imidazol-4-yl))-N-(1-methyl-1H-imidazol-2-ylmethyl))-1-acetyl)-N-(phenylmethyl), (7). Compound **6** (1.07 g) was dissolved in anhydrous DMF (30 cm^3) under inert atmosphere. Solid 2-(chloromethyl)-1-methyl-1H-imidazole dihydrochloride,¹⁰⁶ (590 mg, 3.53 mmol) and K_2CO_3 (2.22 g, 16.0 mmol) were poured into the solution. The reaction was warmed for 12 h at 80 °C. The ESI-MS analysis on the solution showed that the disubstituted product was obtained, but also other by-products were formed, such as monosubstituted intermediate and over-substituted compounds (quaternary ammonium salts). The solvent was removed and the dark brown oil was purified by chromatography on neutral alumina (3 \times 15 cm) with eluent dichloromethane–methanol (98:2–90:10, v/v). Light orange oil (635 mg, 46%) was obtained. $[\alpha]_D^{22}$ ($T = 293$ K) = -20.58 ($c = 5.69 \times 10^{-3}$ M in CHCl_3). Found: C, 59.35; H, 6.61; N, 21.14; M^+ , 854. $\text{C}_{42}\text{H}_{55}\text{N}_{13}\text{O}_7$ requires C, 59.11; H, 6.50; N, 21.34; M , 853.4. UV-vis $\lambda_{\text{max}}(\text{CH}_3\text{CN})/\text{nm}$ 201sh ($\epsilon/\text{dm}^3 \text{ mol}^{-1} \text{ cm}^{-1}$ 9100), 206 (10 220), 210 (10 820), 221 (26 430), 261sh (2870), 291 (2460), 336sh (1830).

CD $\lambda_{\max}(\text{CH}_3\text{CN})/\text{nm}$ 213 ($\Delta\epsilon/\text{dm}^3 \text{ mol}^{-1} \text{ cm}^{-1}$ -3.9), 225 (-2.0), 233 (-1.2), 242sh (-1.0), 255sh (-0.2). ^1H NMR (400 MHz, CDCl_3 , Me_4Si , 298 K): $\delta(\text{ppm})$ 2.50–3.50 (m, 10H, CH_2), 3.57 (s, 4H, CH_2), 3.58 (s, 6H, CH_3), 3.61 (s, 6H, CH_3), 3.70 (m, 2H, CH), 3.75 (s, 6H, CH_3), 3.80 (s, 4H, CH_2), 4.39 (d, 2H, $^3J = 5.6 \text{ Hz}$, CH_2), 5.13 (m, 1H, CH), 6.45 (s, 2H, CH), 6.65 (d, 1H, $^3J = 5.6 \text{ Hz}$, NH-amide), 6.75 (m, 2H, CH), 7.10 (m, 2H, CH), 7.16–7.30 (m, 5H, CH-phenyl), 7.31 (s, 2H, CH). ^{13}C NMR (100.6 MHz, CDCl_3 , 298 K): $\delta(\text{ppm})$ 31.5, 32.5, 33.2, 40.9, 43.4, 48.7, 49.2, 49.6, 50.8, 51.7, 51.9, 60.8, 61.2, 117.7, 121.4, 125.9, 127.2, 127.4, 128.5, 137.4, 138.2, 138.3, 145.6, 170.1, 171.2, 173.2, 174.2, 174.7.

(S)-2-Piperazinemethanamine,1,4-bis[2-((N-(1-hydroxy-3-(1-methyl-1H-imidazol-4-yl))-2-(S)-propyl)-(N-(1-methyl-1H-imidazol-2-ylmethyl))ethyl]-N-(phenylmethyl), (8). A solution of $\text{BH}_3\cdot\text{Me}_2\text{S}$ (7 cm^3 , 74.4 mmol) in dry THF (7 cm^3) was added dropwise to a solution of compound 7 (635.2 mg, 0.744 mmol) in refluxing, dry THF (10 cm^3) under an inert atmosphere. Then, the solvent and Me_2S were slowly distilled for further 5 h while fresh, dry THF (80 cm^3) was added. The solvent was removed under vacuum and the solid residue was taken up with a saturated solution of HCl in methanol (50 cm^3). The solution was refluxed under stirring for 1 h and, after cooling, the solvent was evaporated and the residue was saturated with gaseous ammonia in dry, cooled (0 °C) dichloromethane (50 cm^3). The solid precipitate was separated and treated again with cooled (0 °C) gaseous ammonia saturated dichloromethane. After filtration, the solid residue was submitted again to this treatment. Then the filtrates were combined and, after evaporation, afforded compound 8 (440.6 mg, 78%), which was used in the subsequent reaction without any further purification. $[\alpha]_{\text{D}}^{22}$ ($T = 293 \text{ K}$) = +8.17 ($c = 8.10 \times 10^{-3} \text{ M}$, CHCl_3). Found: C, 63.66; H, 8.19; N, 23.97; M^+ , 756. $\text{C}_{40}\text{H}_{61}\text{N}_{13}\text{O}_2$ requires C, 63.55; H, 8.13; N, 24.09; M , 756.0. UV-vis $\lambda_{\max}(\text{CH}_3\text{CN})/\text{nm}$ 210 ($\epsilon/\text{dm}^3 \text{ mol}^{-1} \text{ cm}^{-1}$ 1140), 221 (1630), 240 (3900), 302sh (230), 315sh (195), 342sh (165). CD $\lambda_{\max}(\text{CH}_3\text{CN})/\text{nm}$ 207 ($\Delta\epsilon/\text{dm}^3 \text{ mol}^{-1} \text{ cm}^{-1}$ -4.3), 216sh (-1.3), 222 (+1.0), 230 (+0.5). ^1H NMR (400 MHz, CDCl_3 , Me_4Si , 298 K): $\delta(\text{ppm})$ 1.65 (m, 4H, CH_2), 2.10–2.60 (m, 16H, CH_2), 2.80 (m, 1H, CH), 2.82 (m, 2H, CH), 3.62 (s, 12H, CH_3), 3.68 (m, 8H, CH_2), 3.86 (s, 2H, CH_2), 4.26 (s, 1H, NH), 6.68 (s, 2H, CH), 6.83 (s, 2H, CH), 6.89 (s, 2H, CH), 7.31 (s, 2H, CH), 7.22–7.41 (m, 5H, CH-phenyl). ^{13}C NMR (100.6 MHz, CDCl_3 , 298 K): $\delta(\text{ppm})$ 29.6, 29.7, 30.1, 42.3, 45.4, 47.0, 47.7, 48.2, 48.8, 49.3, 50.3, 56.3, 62.3, 117.6, 121.6, 126.8, 127.3, 127.8, 128.4, 137.1, 140.0, 146.3, 152.2.

(S)-2-Piperazinemethanamine,1,4-bis[2-((N-(1-acetoxy-3-(1-methyl-1H-imidazol-4-yl))-2-(S)-propyl)-(N-(1-methyl-1H-imidazol-2-ylmethyl))ethyl]-N-(phenylmethyl)-N-(acetoxy)-, also named (S)-Pz-(C2-(HisIm))₂, (9, L). Compound 8 (400 mg, 0.529 mmol) was stirred at room temperature for 6 h in freshly distilled acetic anhydride (10 cm^3) in the presence of 4-dimethylaminopyridine (DMAP, 60 mg, 0.529 mmol). The solution was then evaporated and the residue was purified by flash silica chromatography (3 \times 15 cm), in the following conditions: pressure 2 in min^{-1} , eluent *tert*-butyl methyl ether-*iso*-propanol (50:40, v/v) and an increasing amount of aqueous ammonia (from 1% to 20%). Yellow oil (174 mg, 37%) was obtained. $[\alpha]_{\text{D}}^{22}$ ($T = 293 \text{ K}$) = -7.95 ($c = 4.99 \times 10^{-3} \text{ M}$ in CHCl_3). Found:

C, 62.34; H, 7.76; N, 20.51; M^+ , 883. $\text{C}_{46}\text{H}_{67}\text{N}_{13}\text{O}_5$ requires C, 62.63; H, 7.66; N, 20.64; M , 882.1. UV-vis $\lambda_{\max}(\text{CH}_3\text{CN})/\text{nm}$ 207 ($\epsilon/\text{dm}^3 \text{ mol}^{-1} \text{ cm}^{-1}$ 2210), 212 (2040), 219 (2840), 236 (5610), 238 (5705), 253sh (1660), 265sh (1205), 292 (1130), 302sh (1040), 336sh (330), 351sh (300), 369sh (260), 382sh (180). CD $\lambda_{\max}(\text{CH}_3\text{CN})/\text{nm}$ 209 ($\Delta\epsilon/\text{dm}^3 \text{ mol}^{-1} \text{ cm}^{-1}$ -3.2), 215 (-2.9), 225 (+0.2), 231 (-0.4), 244 (+0.1). ^1H NMR (400 MHz, CDCl_3 , Me_4Si , 298 K): $\delta(\text{ppm})$ 1.95–2.00 (s, 9H, CH_3), 2.35–2.75 (m, 22H, CH_2), 3.30 (m, 3H, CH), 3.58 (s, 12H, CH_3), 3.80 (s, 4H, CH_2), 4.06 (m, 4H, CH_2), 6.60 (s, 2H, CH), 6.75 (m, 2H, CH), 7.10 (m, 2H, CH), 7.28 (s, 2H, CH), 7.14–7.32 (m, 5H, CH-phenyl). ^{13}C NMR (100.6 MHz, CDCl_3 , 298 K): $\delta(\text{ppm})$ 20.6, 20.8, 21.7, 26.4, 32.5, 33.5, 38.9, 42.3, 47.0, 47.7, 48.2, 48.8, 49.3, 49.6, 56.7, 60.4, 64.1, 117.3, 117.8, 121.4, 125.9, 127.1, 127.3, 127.8, 128.4, 128.8, 136.5, 137.5, 139.5, 145.6, 170.6, 171.4, 171.7.

Synthesis of the copper(II) complexes

$[\text{Cu}_2(\text{L})][\text{ClO}_4]_4\cdot 4\text{H}_2\text{O}$. The ligand (S)-Pz-(C2-(HisIm))₂ (0.053 g, 0.060 mmol) was dissolved in MeCN (8 cm^3) yielding a shining yellow solution. Then, copper(II) perchlorate hexahydrate in methanol (0.12 mmol), from a 0.0975 $\text{dm}^3 \text{ mol}^{-1} \text{ cm}^{-1}$ stock solution, was added dropwise and a color change from yellow to shining green was observed. The solution was stirred at room temperature for 4 h, and then reduced to a small volume (~2 cm^3) and treated with diethyl ether (5 cm^3). The product precipitated by cooling in ice bath and was allowed to stand overnight at 0 °C. Then, the green solid precipitate formed was filtered, washed with diethyl ether (3 \times 1 cm^3) and dried under vacuum. Yield 79%. Found: C, 37.26; H, 5.27; N, 12.25; Cu, 8.61; M^+ , 1479. $\text{C}_{46}\text{H}_{67}\text{N}_{13}\text{O}_{21}\text{Cu}_2\text{Cl}_4\cdot 4\text{H}_2\text{O}$ requires C, 37.35; H, 5.11; N 12.31, Cu, 8.59; M , 1479.1. UV-vis $\lambda_{\max}(\text{CH}_3\text{CN})/\text{nm}$ 210 ($\epsilon/\text{dm}^3 \text{ mol}^{-1} \text{ cm}^{-1}$ 42 300), 292 (2750), 646 (90). CD $\lambda_{\max}(\text{CH}_3\text{CN})/\text{nm}$ 213 ($\Delta\epsilon/\text{dm}^3 \text{ mol}^{-1} \text{ cm}^{-1}$ -6.80), 224sh (-3.82), 290 (+1.24), 486 (+0.01), 614 (-0.08).

$[\text{Cu}_3(\text{L})][\text{ClO}_4]_6\cdot 6\text{H}_2\text{O}$. The ligand (S)-Pz-(C2-(HisIm))₂ (0.058 g, 0.066 mmol) was dissolved at room temperature in MeCN (10 cm^3) yielding a shining yellow solution. Then, copper(II) perchlorate hexahydrate in methanol (0.22 mmol), from a 0.0975 $\text{dm}^3 \text{ mol}^{-1} \text{ cm}^{-1}$ stock solution, was added dropwise and a color change from yellow to dark blue was observed. The solution was warmed up to reflux for 6 h, and then it was rotary-evaporated to a small volume (2 cm^3) and treated with diethyl ether (5 cm^3). The product precipitated by cooling in ice bath and was allowed to stand overnight at 0 °C. Then, the light grey solid was filtered, washed with diethyl ether (3 \times 1 cm^3) and dried under vacuum. Yield 75%. Found: C, 30.92; H, 4.49; N, 10.15; Cu, 10.83; M^+ , 1777. $\text{C}_{46}\text{H}_{67}\text{N}_{13}\text{O}_{29}\text{Cu}_3\text{Cl}_6\cdot 6\text{H}_2\text{O}$ requires C, 31.08; H, 4.48; N 10.24; Cu, 10.72; M , 1777.5. UV-vis $\lambda_{\max}(\text{CH}_3\text{CN})/\text{nm}$ 211 ($\epsilon/\text{dm}^3 \text{ mol}^{-1} \text{ cm}^{-1}$ 57 000), 233sh (32 000), 292 (5200), 661 (20). CD $\lambda_{\max}(\text{CH}_3\text{CN})/\text{nm}$ 224 ($\Delta\epsilon/\text{dm}^3 \text{ mol}^{-1} \text{ cm}^{-1}$ -6.81), 233 (-0.07), 289 (+0.21), 614 (-0.02).

Caution! Perchlorate complexes with organic ligands are potentially explosive and should be handled with great care. Only small amounts of material should be prepared. We did not have problems working with small amounts of the perchlorate complexes described in this paper.

Acknowledgements

GZ thanks the support from the Marie Curie Intra-European Fellowship within the 7th European Community Framework Programme (PIEF-GA-2009-235237), KKA the Research Council of Norway (Grant 177661/V30), MFI thanks the Norwegian Research Council through a Center of excellence Grant (179568/V30) and The Norwegian Supercomputing Programme. MFI thanks Prof. Trygve Helgaker (CTCC, University of Oslo) for fruitful discussions. LC thanks the Italian MIUR (through a PRIN project), CIRCMSB and the University of Pavia for support. Stefano Pandini is acknowledged for ESI-MS analysis.

References

- 1 A. Messerschmidt, in *Multicopper Oxidases*, World Scientific, Singapore, 1997.
- 2 J. Reedijk, and E. Bowman, in *Bioinorganic Catalysis*, 2nd edn., Marcel Dekker, New York, 1999.
- 3 G. Battaini, A. Granata, E. Monzani, M. Gullotti and L. Casella, *Adv. Inorg. Chem.*, 2006, **58**, 185–233.
- 4 E. I. Solomon, E. I. Sundaram and T. E. Machonkin, *Chem. Rev.*, 1996, **96**, 2563–2605.
- 5 Y. Matoba, T. Kumagai, A. Yamamoto, H. Yoshitsu and M. Sugiyama, *J. Biol. Chem.*, 2006, **281**, 8981–8990.
- 6 J. Yoon, S. Fujii and E. I. Solomon, *Proc. Natl. Acad. Sci. U. S. A.*, 2009, **106**, 6585–6590.
- 7 C. Eicken, F. Zippel, K. Büldt-Karentzopoulos and B. Krebs, *FEBS Lett.*, 1998, **436**, 293–299.
- 8 T. Klabunde, C. Eicken, J. C. Sacchettini and B. Krebs, *Nat. Struct. Biol.*, 1998, **5**, 1084–1090.
- 9 C. Gerdemann, C. Eicken and B. Krebs, *Acc. Chem. Res.*, 2002, **35**, 183–191.
- 10 T. Bertrand, C. Jolivat, P. Briozzo, E. Caminade, N. Joly, C. Madzak and C. Mougin, *Biochemistry*, 2002, **41**, 7325–7333.
- 11 A. Messerschmidt, H. Luecke and H. Huber, *J. Mol. Biol.*, 1993, **230**, 997–1014.
- 12 S. Koikeda, K. Ando, H. Kaji, T. Inoue, S. Murao, K. Takeuchi and T. Samejima, *J. Biol. Chem.*, 1993, **268**, 18801–18809.
- 13 A. Shimizu, T. Samejima, S. Hirota, S. Yamaguchi, N. Sakurai and T. Sakurai, *J. Biochem.*, 2003, **133**, 767–772.
- 14 G. Zoppellaro, N. Sakurai, K. Kataoka and T. Sakurai, *Biosci., Biotechnol., Biochem.*, 2004, **68**, 1998–2000.
- 15 T. Sakurai and K. Kataoka, *Cell. Mol. Life Sci.*, 2007, **64**, 2642–2656.
- 16 J. A. Fee, in “Copper Proteins-Systems Containing the “Blue” Copper Center”, ed. J. D. Dunitz, P. Hemmerich, R. H. Holm, J. A. Ibers, C. K. Jørgensen, J. B. Neilands, D. Reinen and R. J. P. Williams, *Structure and Bonding*, Springer, Berlin, 1975, **23**, pp. 1–60.
- 17 R. Cardenas-Vazquez, O. Yokosuka and B. H. Billing, *Biochem. J.*, 1986, **236**, 625–633.
- 18 I. Bento, L. O. Martins, G. G. Lopes, M. A. Carrondo and P. F. Lindley, *Dalton Trans.*, 2005, 3507–3513.
- 19 L. Casella, M. Gullotti, L. Santagostini, G. Zoppellaro and T. Sakurai, *J. Inorg. Biochem.*, 2006, **100**, 2127–2139.
- 20 S. Shipovskov, H. Q. Nimal Gunaratne, K. R. Seddon and G. Stephens, *Green Chem.*, 2008, **10**, 806–810.
- 21 M. A. Tadesse, A. D’Annibale, C. Galli, P. Gentili and F. Sergi, *Org. Biomol. Chem.*, 2008, **6**, 868–878.
- 22 L. Quintanar, M. Gebhard, T. P. Wang, D. J. Kosman and E. I. Solomon, *J. Am. Chem. Soc.*, 2004, **126**, 6579–6589.
- 23 T. J. Lawton, L. A. Sayavedra-Soto, D. J. Arp and A. C. Rosenzweig, *J. Biol. Chem.*, 2009, **284**, 10174–10180.
- 24 Y. Matoba, T. Kumagai, A. Yamamoto, H. Yoshitsu and M. Sugiyama, *J. Biol. Chem.*, 2006, **281**, 8981–8990.
- 25 H. Decker, T. Schweikardt and F. Tuczek, *Angew. Chem., Int. Ed.*, 2006, **45**, 4546–4550.
- 26 I. Bento, C. Peixoto, V. N. Zaitsev and P. F. Lindley, *Acta Crystallogr., Sect. D: Biol. Crystallogr.*, 2007, **63**, 240–248.
- 27 V. Ducros, A. M. Brzozowski, K. S. Wilson, S. H. Brown, P. Østergaard, P. Schneider, D. S. Yaver, A. H. Pedersen and G. J. Davies, *Nat. Struct. Biol.*, 1998, **5**, 310–316.
- 28 K. Piontek, M. Antorini and T. Choinowski, *J. Biol. Chem.*, 2002, **277**, 37663–37669.
- 29 A. Messerschmidt, R. Ladenstein, R. Huber, M. Bolognesi, L. Avigliano, R. Petruzzelli, A. Rossi and A. Finazzi-Agrò, *J. Mol. Biol.*, 1992, **224**, 179–205.
- 30 I. Zaitseva, V. Zaitsev, G. Card, K. Moshkov, B. Bax, A. Ralph and P. Lindley, *J. Biol. Inorg. Chem.*, 1996, **1**, 15–23.
- 31 S. Roberts, A. Weichsel, G. Grass, K. Thakali, J. Hazzard, G. Tollin, C. Rensing and W. Montfort, *Proc. Natl. Acad. Sci. U. S. A.*, 2002, **99**, 2766–2771.
- 32 K. Kataoka, R. Sugiyama, S. Hirota, K. Urata, Y. Minagawa, D. Seo and T. Sakurai, *J. Biol. Chem.*, 2009, **284**, 14405–14413.
- 33 E. I. Solomon, A. J. Augustine and J. Yoon, *Dalton Trans.*, 2008, (30), 3921–3932.
- 34 U. Ryde, Y. W. Hsiao, L. Rulisek and E. I. Solomon, *J. Am. Chem. Soc.*, 2007, **129**, 726–727.
- 35 L. Quintanar, J. J. Yoon, C. P. Aznar, A. E. Palmer, K. K. Andersson, R. D. Britt and E. I. Solomon, *J. Am. Chem. Soc.*, 2005, **127**, 13832–13845.
- 36 A. E. Palmer, S. K. Lee and E. I. Solomon, *J. Am. Chem. Soc.*, 2001, **123**, 6591–6599.
- 37 H. W. Huang, G. Zoppellaro and T. Sakurai, *J. Biol. Chem.*, 1999, **274**, 32718–32724.
- 38 G. Zoppellaro, H. W. Huang and T. Sakurai, *Inorg. React. Mech.*, 2000, **2**, 79–84.
- 39 G. Zoppellaro, T. Sakurai and H. W. Huang, *J. Biochem.*, 2001, **129**, 949–953.
- 40 L. E. Andréasson, R. Brändén and B. Reinhammar, *Biochim. Biophys. Acta*, 1976, **438**, 370–379.
- 41 L. E. Andréasson and B. Reinhammar, *Biochim. Biophys. Acta*, 1979, **568**, 145–156.
- 42 K. D. Karlin, Y. Gultneh, T. Nicholson and J. Zubieta, *Inorg. Chem.*, 1985, **24**, 3725–3727.
- 43 J. Reim and B. Krebs, *J. Chem. Soc., Dalton Trans.*, 1997, 3793–3804.
- 44 C. Fernandes, A. Neves, A. J. Bortoluzzi, A. S. Mangrich, E. Rentschler, B. Szpoganicz and E. Schwingel, *Inorg. Chim. Acta*, 2001, **320**, 12–21.
- 45 A. E. Lewis and W. B. Tolman, *Chem. Rev.*, 2004, **104**, 1047–1076.
- 46 I. A. Koval, K. Selmeçci, C. Belle, C. Philouze, E. Saint-Aman, I. Gautier-Luneau, A. M. Schuitema, M. van Vliet, P. Gamez, O. Roubeau, M. Lützen, B. Krebs, M. Lutz, A. L. Spek, J. L. Pierre and J. Reedijk, *Chem.-Eur. J.*, 2006, **12**, 6138–6150.
- 47 Y. Funahashi, T. Nishikawa, Y. Wasada-Tsutsui, Y. Kajita, S. Yamaguchi, H. Arai, T. Ozawa, K. Jitsukawa, T. Tosha, S. Hirota, T. Kitagawa and Masuda, *J. Am. Chem. Soc.*, 2008, **130**, 16444–16445.
- 48 K. S. Banu, T. Chattopadhyay, A. Banerjee, S. Battacharya, E. Suresh, M. Nethaji, E. Zangrando and D. Das, *Inorg. Chem.*, 2008, **47**, 7083–7093.
- 49 P. A. Cole, D. E. Root, P. Mukherjee, E. I. Solomon and T. D. P. Stack, *Science*, 1996, **273**, 1848–1850.
- 50 H. Adams, N. A. Bailey, M. J. S. Dwyer, D. E. Fenton, P. C. Hellier, P. D. Hempstead and J.-M. Latour, *J. Chem. Soc., Dalton Trans.*, 1993, 1207–1216.
- 51 P. Chaudhuri, I. Karpenstein, M. Winter, C. Butzlaff, E. Bill, A. X. Trautwein, U. Flörke and H.-J. Haupt, *J. Chem. Soc., Chem. Commun.*, 1992, 321–322.
- 52 S. Meenakumari, S. K. Tiwary and A. R. Chakravarty, *Inorg. Chem.*, 1994, **33**, 2085–2089.
- 53 B. Graham, L. Spiccia, G. D. Fallon, M. T. W. Hearn, F. E. Mabbs, B. Mubarak and K. S. Murray, *J. Chem. Soc., Dalton Trans.*, 2002, 1226–1232.
- 54 A. Mukherjee, I. Rudra, S. G. Naik, M. Nethaji, S. Ramasesha and A. R. Chakravarty, *Inorg. Chem.*, 2003, **42**, 5660–5668.
- 55 S. Gupta, A. Mukherjee, M. Nethaji and A. R. Chakravarty, *Polyhedron*, 2004, **23**, 643–647.
- 56 (a) W. B. Tolman, *J. Biol. Inorg. Chem.*, 2006, **11**, 261–271; (b) V. Nanda and R. L. Koder, *Nat. Chem.*, 2010, **2**, 15–24.
- 57 B. L. Feringa, in *Bioinorganic Chemistry of Copper*, ed. K. D. Karlin and Z. Tyeklar, Chapman & Hall, New York, 1993, pp. 306–324.
- 58 L. Santagostini, M. Gullotti, R. Pagliarin, E. Bianchi, L. Casella and E. Monzani, *Tetrahedron: Asymmetry*, 1999, **10**, 281–295.
- 59 M. C. Mimmi, M. Gullotti, L. Santagostini, A. Saladino, L. Casella, E. Monzani and R. Pagliarin, *J. Mol. Catal. A: Chem.*, 2003, **204–205**, 381–389.

- 60 M. C. Mimmi, M. Gullotti, L. Santagostini, R. Pagliarin, L. De Gioia, E. Monzani and L. Casella, *Eur. J. Inorg. Chem.*, 2003, 3934–3944.
- 61 L. Santagostini, M. Gullotti, R. Pagliarin, E. Monzani and L. Casella, *Chem. Commun.*, 2003, 2186–2187.
- 62 M. Gullotti, L. Santagostini, R. Pagliarin, S. Palavicini, L. Casella, E. Monzani and G. Zoppellaro, *Eur. J. Inorg. Chem.*, 2008, 2081–2089.
- 63 M. C. Mimmi, M. Gullotti, L. Santagostini, G. Battaini, E. Monzani, R. Pagliarin, G. Zoppellaro and L. Casella, *Dalton Trans.*, 2004, (14), 2192–2201.
- 64 M. Gullotti, L. Santagostini, R. Pagliarin, A. Granata and L. Casella, *J. Mol. Catal. A: Chem.*, 2005, **235**, 271–284.
- 65 F. G. Mutti, R. Pievo, M. Sgobba, M. Gullotti and L. Santagostini, *Bioinorg. Chem. Applic.*, **2008**, DOI: 10.1155/2008/762029, Article ID 762029.
- 66 F. G. Mutti, G. Zoppellaro, M. Gullotti, L. Santagostini, R. Pagliarin, K. K. Andersson and L. Casella, *Eur. J. Inorg. Chem.*, 2009, 554–566.
- 67 L. Casella, M. Gullotti, G. Pallanza and M. Buga, *Inorg. Chem.*, 1991, **30**, 221–227.
- 68 E. Monzani, L. Casella, G. Zoppellaro, M. Gullotti, R. Pagliarin, R. P. Bonomo, G. Tabbi, G. Nardin and L. Randaccio, *Inorg. Chim. Acta*, 1998, **282**, 180–192.
- 69 J. E. Pate, P. K. Ross, T. J. Thamann, C. A. Reed, K. D. Karlin, N. T. Sorrell and E. I. Solomon, *J. Am. Chem. Soc.*, 1989, **111**, 5198–5205.
- 70 H. Yokoi and W. Addison, *Inorg. Chem.*, 1977, **16**, 1341–1349.
- 71 S. K. Hoffmann and J. Goslar, *J. Solid State Chem.*, 1982, **44**, 343–353.
- 72 R. H. Holm, P. Kennepohl and E. I. Solomon, *Chem. Rev.*, 1996, **96**, 2239–2314.
- 73 Y. Funahashi, K. Nakaya, S. Hirota and O. Yamauchi, *Chem. Lett.*, 2000, **29**, 1172–1173.
- 74 Y.-M. Lee, Mi-A. Kwon, S. K. Kang, J. H. Jeong and S.-N. Choi, *Inorg. Chem. Commun.*, 2003, **6**, 197–201.
- 75 J. Peisach and W. E. Blumberg, *Arch. Biochem. Biophys.*, 1974, **165**, 691–708.
- 76 J. R. Pilbrow, “High Spin Systems” in *Foundations of Modern EPR*, ed. G. R. Eaton, S. S. Eaton and K. M. Salikhov, World Sci., 1998, pp. 185–195.
- 77 A. J. Weil, J. R. Bolton and J. E. Wertz, in *Electron Paramagnetic Resonance: Elementary Theory and Practical Applications*, Wiley-Interscience, 2nd Edition, 1993, ch. 6.
- 78 (a) A. Bencini and D. Gatteschi, in *EPR of Exchange Coupled Systems*, Springer-Verlag, Berlin, 1990; (b) *Magnetism: A Supramolecular Function*, ed. O. Kahn, NATO ASI Series C, **484**, Kluwer, Dordrecht, 1996.
- 79 W. L. Driessen, F. B. Hulsbergen, J. Reedijk and G. C. Verschoor, *Transition Met. Chem.*, 1985, **10**, 390–392.
- 80 G. Battaini, L. Casella, M. Gullotti, E. Monzani, G. Nardin, A. Perotti, L. Randaccio, L. Santagostini, F. W. Heinemann and S. Schindler, *Eur. J. Inorg. Chem.*, 2003, 1197–1205.
- 81 M. L. Mirica, X. Ottenwaelde and T. D. P. Stack, *Chem. Rev.*, 2004, **104**, 1013–1045.
- 82 L. Rulišėk and J. Vondrášek, *J. Inorg. Biochem.*, 1998, **71**, 115–127.
- 83 G. Eisenhoffer, I. J. Kopin and D. S. Goldstein, *Pharmacol. Rev.*, 2004, **56**, 331–349.
- 84 T. Schewe, Y. Steffen and H. Sies, *Arch. Biochem. Biophys.*, 2008, **476**, 102–106.
- 85 E. Monzani, G. Battaini, A. Perotti, L. Casella, M. Gullotti, L. Santagostini, G. Nardin, L. Randaccio, S. Geremia, P. Zanello and G. Opromolla, *Inorg. Chem.*, 1999, **38**, 5359–5369.
- 86 R. Noyori, *Angew. Chem., Int. Ed.*, 2002, **41**, 2008–2022.
- 87 P. Barbaro, C. Bianchini, G. Giambastiani and S. L. Parisel, *Coord. Chem. Rev.*, 2004, **248**, 2131–2150; M. S. Taylor and E. N. Jacobsen, *Proc. Natl. Acad. Sci. U. S. A.*, 2004, **101**, 5368–5373.
- 88 J. P. Klinman, *Chem. Rev.*, 1996, **96**, 2541–2561; N. J. Blackburn, R. W. Strange, R. T. Carr and S. J. Benkovic, *Biochemistry*, 1992, **31**, 5298–5303; N. J. Blackburn, S. S. Hasnain, T. M. Pettingill and R. W. Strange, *J. Biol. Chem.*, 1991, **266**, 23120–23127.
- 89 S. T. Prigge, A. S. Kolhekar, B. A. Eipper, R. E. Mains and L. M. Amzel, *Science*, 1997, **278**, 1300–1305; S. T. Prigge, A. S. Kolhekar, B. A. Eipper, R. E. Mains and L. M. Amzel, *Nat. Struct. Biol.*, 1999, **6**, 976–983; S. T. Prigge, B. A. Eipper, R. E. Mains and L. M. Amzel, *Science*, 2004, **304**, 864–867; P. Chen and E. I. Solomon, *J. Am. Chem. Soc.*, 2004, **126**, 4991–5000; P. Chen, J. Bell, B. A. Eipper and E. I. Solomon, *Biochemistry*, 2004, **43**, 5735–5747.
- 90 R. J. Deeth, A. Anastasi, C. Diedrich and K. Randell, *Coord. Chem. Rev.*, 2009, **253**, 795–816.
- 91 R. J. Deeth and L. J. A. Hearnshaw, *Dalton Trans.*, 2005, 3638–3645.
- 92 *Spartan 08 (V1.2.0)*, Wavefunction Inc., Irvine, CA 92612, USA.
- 93 P. A. M. Dirac, *Proc. R. Soc. London, Ser. A*, 1929, **123**, 714–733.
- 94 J. C. Slater, *Phys. Rev.*, 1951, **81**, 385–392.
- 95 S. H. Vosko, L. Wilk and M. Nusair, *Can. J. Phys.*, 1980, **58**, 1200–1211.
- 96 A. D. Becke, *Phys. Rev. A: At., Mol., Opt. Phys.*, 1988, **38**, 3098–3100.
- 97 J. P. Perdew, *Phys. Rev. B*, 1986, **33**, 8822–8824.
- 98 A. Schäfer, C. Huber and R. Ahlrichs, *J. Chem. Phys.*, 1994, **100**, 5829–5835.
- 99 K. Eichkorn, O. Treutler, H. Öhm, M. Häser and R. Ahlrichs, *Chem. Phys. Lett.*, 1995, **242**, 652–660.
- 100 M. Sierka, A. Hogekamp and R. Ahlrichs, *J. Chem. Phys.*, 2003, **118**, 9136–9148.
- 101 M. V. Arnim and R. Ahlrichs, *J. Chem. Phys.*, 1999, **111**, 9183–9190.
- 102 M. Dolg, U. Wedig, H. Stoll and H. Preuss, *J. Chem. Phys.*, 1987, **86**, 866–872.
- 103 T. A. Halgren, *J. Comput. Chem.*, 1996, **17**, 490–519; T. A. Halgren, *J. Comput. Chem.*, 1996, **17**, 520–552; T. A. Halgren, *J. Comput. Chem.*, 1996, **17**, 553–586; T. A. Halgren and R. B. Nachbar, *J. Comput. Chem.*, 1996, **17**, 587–615; T. A. Halgren, *J. Comput. Chem.*, 1996, **17**, 616–641; T. A. Halgren, *J. Comput. Chem.*, 1999, **20**, 720–729; T. A. Halgren, *J. Comput. Chem.*, 1999, **20**, 730–748.
- 104 S. Groszkowski, J. Sienkiewicz, L. Majman, R. Oteleanu and M. Retexeanu, *J. Med. Chem.*, 1968, **11**(3), 621–622.
- 105 A. Noordam, L. Maat and H. C. Beyerman, *Rec. J. R. Netherlands Chem. Soc.*, 1978, **97**, 293–295.
- 106 L. Casella, O. Carugo, M. Gullotti, S. Garofani and P. Zanello, *Inorg. Chem.*, 1993, **32**, 2056–2067.